Molecular Therapy
Original Article

SOCS3 regulates pathological retinal angiogenesis through modulating SPP1 expression in microglia and macrophages

Tianxi Wang,[1] Satoshi Kaneko,[1] Emil Kriukov,[2] David Alvarez,[3] Enton Lam,[1] Yidi Wang,[3] Sara La Manna,[4] Daniela Marasco,[4] Angeles Fernandez-Gonzalez,[5] S. Alex Mitsialis,[5] Stella Kourembanas,[5] Andreas Stahl,[6] Mei Chen,[7] Heping Xu,[7] Petr Baranov,[2] Guoshuai Cai,[8] Ulrich H. von Andrian,[3,9] and Ye Sun[1]

[1]Department of Ophthalmology, Boston Children's Hospital, Harvard Medical School, Boston, MA 02115, USA; [2]Department of Ophthalmology, The Schepens Eye Research Institute of Massachusetts Eye and Ear, Harvard Medical School, Boston, MA 02114, USA; [3]Department of Immunology and HMS Center for Immune Imaging, Harvard Medical School, Boston, MA 02115, USA; [4]Department of Pharmacy, University of Naples "Federico II", 80138 Naples, Italy; [5]Division of Newborn Medicine, Department of Pediatrics, Boston Children's Hospital, Harvard Medical School, Boston, MA 02115, USA; [6]Department of Ophthalmology, University Medicine Greifswald, 17475 Greifswald, Germany; [7]Centre for Experimental Medicine, School of Medicine, Dentistry and Biomedical Sciences, Queen's University Belfast, Belfast, UK; [8]Department of Surgery, College of Medicine, University of Florida, Gainesville, FL 32610, USA; [9]The Ragon Institute of MGH, MIT, and Harvard, Cambridge, MA 02139, USA

Pathological ocular angiogenesis has long been associated with myeloid cell activation. However, the precise cellular and molecular mechanisms governing the intricate crosstalk between the immune system and vascular changes during ocular neovascularization formation remain elusive. In this study, we demonstrated that the absence of the suppressor of cytokine signaling 3 (SOCS3) in myeloid cells led to a substantial accumulation of microglia and macrophage subsets during the neovascularization process. Our single-cell RNA sequencing data analysis revealed a remarkable increase in the expression of the secreted phosphoprotein 1 (*Spp1*) gene within these microglia and macrophages, identifying subsets of *Spp1*-expressing microglia and macrophages during neovascularization formation in angiogenesis mouse models. Notably, the number of *Spp1*-expressing microglia and macrophages exhibited further elevation during neovascularization in mice lacking myeloid SOCS3. Moreover, our investigation unveiled the *Spp1* gene as a direct transcriptional target gene of signal transducer and activator of transcription 3. Importantly, pharmaceutical activation of SOCS3 or blocking of SPP1 resulted in a significant reduction in pathological neovascularization. In conclusion, our study highlights the pivotal role of the SOCS3/STAT3/SPP1 axis in the regulation of pathological retinal angiogenesis.

INTRODUCTION

The neurovascular unit serves as a fundamental functional module crucial for maintaining overall health within the central nervous system (CNS), including the retina.[1] Recent findings strongly underscore the pivotal role of preserving neurovascular health in supporting the well-being of the entire CNS.[2] Within the CNS, myeloid cells play a central role in shaping blood vessel development[3] and maintaining vascular integrity, particularly in response to various injuries.[4] Neovascularization (NV), the process of forming new blood vessels, is a hallmark of vascular eye diseases such as retinopathy of prematurity (ROP) and neovascular age-related macular degeneration (nAMD), representing the primary cause of vision loss.[5–8] Preterm infants experiencing infections face a significantly heightened risk for neurovascular injury within the retinas.[9–12] In this context, infections, often accompanied by proinflammatory cytokine production, are strongly linked to an increased likelihood of developing retinopathy.[13] In clinical practice, infections and their associated inflammation are common, emphasizing the critical need for a deeper comprehension of the mechanisms driving neurovascular injury in the CNS.[13] While it is clear that inflammation and immune dysfunction play significant roles in the pathogenesis of retinopathies,[9,10,13–16] the precise nature of this connection remains inadequately explored, and effective strategies for managing such inflammation have yet to be definitively established.

The suppressor of cytokine signaling (SOCS) protein family consists of eight members labeled as SOCS1–7 and cytokine inducible SH2 containing protein (CIS). They function to inhibit the activation of signal transducer and activator of transcription (STAT) through Janus tyrosine kinase (JAK)/STAT activating receptors.[17] Among these, SOCS3 emerges as a pivotal player, playing a vital role in preventing inflammatory diseases mediated by interleukin 6 and granulocyte colony-stimulating factor signaling pathways.[18] Its functions intricately link to its ability to modulate tissue inflammation and cytokine

Received 1 November 2023; accepted 15 March 2024;
https://doi.org/10.1016/j.ymthe.2024.03.025.

Correspondence: Ye Sun, Department of Ophthalmology, Boston Children's Hospital, Harvard Medical School, Boston, MA 02115, USA.
E-mail: ye.sun@childrens.harvard.edu

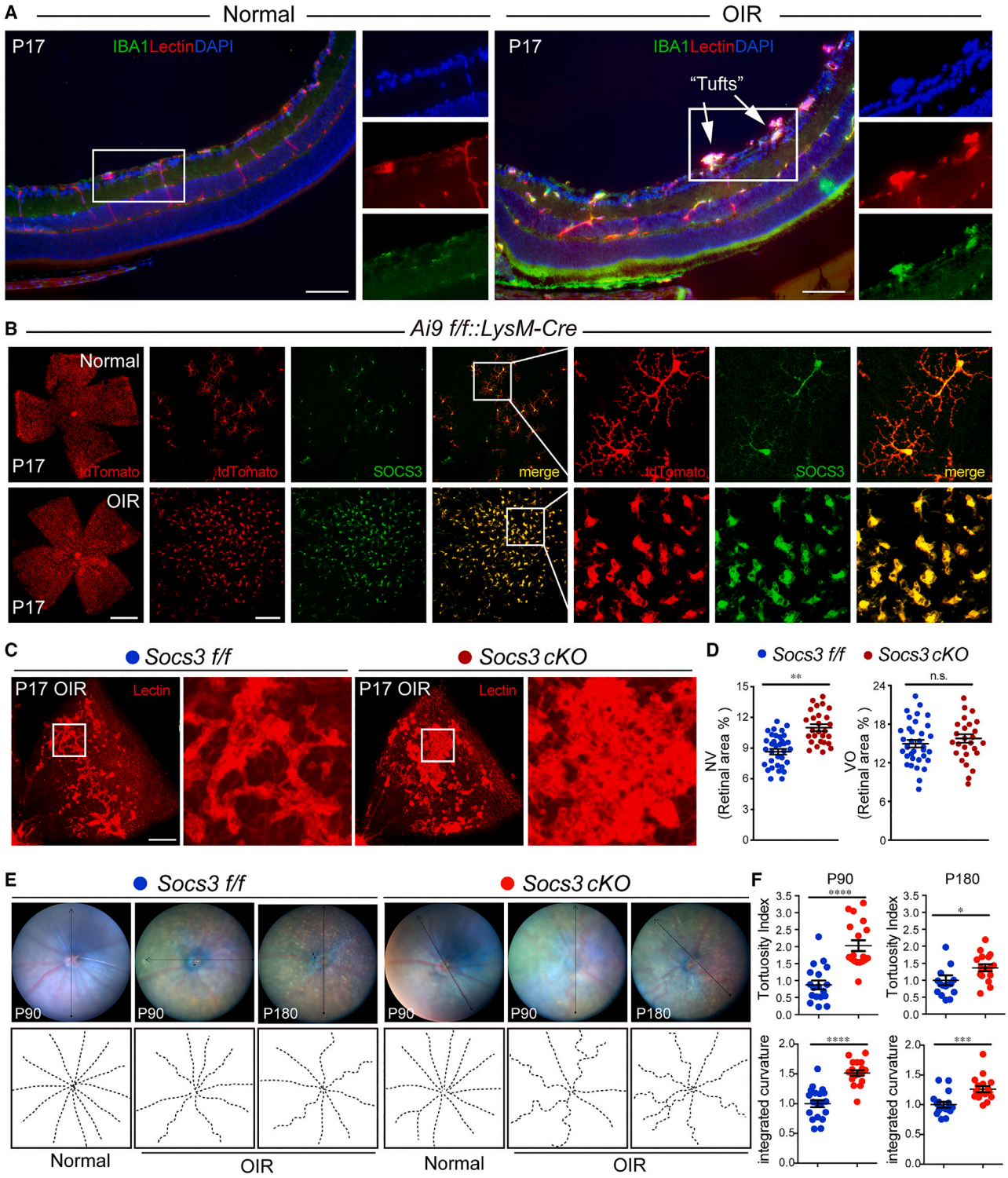

Figure 1. Myeloid cell accumulation and SOCS3 induction during NV formation in OIR retinas

(A) Representative cross-sections of IBA1 (green)- and Lectin (red)-stained normal and OIR retinas from C57BL/6J mice at P17. DAPI (blue) indicates nuclei. White boxes indicate retinal vessel areas or NV areas (n = 6). White arrows point to "Tufts" (NV). Scale bar, 100 μm. (B) Representative flat mounts of SOCS3 (green)-stained normal and OIR retinas from myeloid-specific LysM-Cre driven-Ai9 tdTomato (red) reporter mice at P17 (n = 6). Scale bar, 1,000 μm for flat-mount images, 200 μm for images in columns

(legend continued on next page)

secretion.[19,20] Moreover, SOCS3 exerts a significant influence on pathological ocular angiogenesis.[21–24] In the realm of ocular biology, SOCS3 holds a critical position, impacting various facets of eye health. Notably, endothelial SOCS3 deficiency enhances retinal NV by activating the STAT3 and mammalian target of rapamycin (mTOR) pathways[21] in the context of an ROP mouse model, the oxygen-induced retinopathy (OIR) mice.[25] Our prior research has revealed the role of neuronal and glial SOCS3 in suppressing pathological retinal angiogenesis in OIR mice by targeting vascular endothelial growth factor A (VEGFA).[22] Furthermore, the deletion of SOCS3 effectively abolishes the anti-inflammatory and vaso-protective effects associated with retinoic acid receptor-related orphan receptor alpha deficiency in OIR mice.[23] Additionally, myeloid SOCS3 regulates laser-induced choroidal NV (CNV) by modulating the accumulation of macrophage and microglia.[26] Moreover, the absence of myeloid SOCS3 has been linked to enhanced NV in OIR mice.[24] Consequently, SOCS3 emerges as a crucial regulator of cytokine signaling and inflammation within the eye. Dysregulation of SOCS3 significantly contributes to the pathogenesis of a spectrum of eye diseases, rendering it an important focus of research in the field of ophthalmology. A comprehensive understanding of its functions in both normal eye biology and disease contexts is essential for developing targeted therapies to address vision-threatening conditions.

In our present study, we aimed to elucidate the crucial role of myeloid SOCS3 in the development of NV within the retina. To achieve this, we manipulated both overexpression and deletion of SOCS3 specifically in immune cells of myeloid origin. This allowed us to shed light on the protection role of SOCS3 in the context of pathological retinal angiogenesis and, in parallel, elucidate the augmented accumulation of microglia and macrophages in areas affected by NV due to myeloid SOCS3 deficiency. Subsequently, we delved into the downstream soluble proteins of the SOCS3/STAT3 pathway. Our single-cell RNA sequencing (scRNA-seq) data analysis revealed an increased relative abundance of several clusters of microglia in mice with OIR, especially in those bearing myeloid SOCS3 deficiency. Using scRNA-seq, we identified a microglia subset enriched in OIR mice, particularly in myeloid SOCS3-deficient OIR mice, termed NV-associated microglia (NVAM). Notably, these microglia exhibited high expression of secreted phosphoprotein 1 (SPP1), also known as Osteopontin. SPP1 is a cytokine known to upregulate the expression of interferon-gamma and interleukin-12[27] and is expressed by a subset of microglia and macrophages, T cells, and other immune cells, impacting various macrophage functions, including phagocytosis. Intriguingly, surgically extracted choroidal neovascular membranes from human patients with nAMD exhibit an increase in SPP1 expression, accompanied by numerous SPP1-positive myeloid cells.[28] Our findings provided substantial evidence of a significant induction of SPP1 in the NV areas of both OIR and laser-induced CNV mouse models, particularly in mice lacking myeloid SOCS3. Importantly, the genetic knockout of SPP1 effectively curbed the NV induced by myeloid SOCS3 deficiency in both the ROP and nAMD mouse models. These findings underscored the contributory role of SPP1 in ocular NV development. Moreover, our research uncovered the direct transcriptional regulation of *Spp1* by STAT3. In summary, our results offer a comprehensive picture of how myeloid SOCS3 governs pathological retinal NV by intricately modulating SPP1 expression, thereby highlighting the pivotal role of SPP1 in orchestrating immune-vascular crosstalk during retinal angiogenesis development.

RESULTS

Myeloid cell activation and accumulation during NV development in OIR

In the retinas affected by OIR, an accumulation of ionized calcium-binding adaptor molecule 1 positive ($IBA1^+$) microglia and macrophages was observed around NV sites, identified by Lectin labeling, as opposed to their distribution in normal retinas (Figure 1A). To delve deeper into the involvement of myeloid cells in the OIR development process, we generated myeloid-specific reporter mice. These mice feature a dual-color labeling system (membrane-localized tdTomato and membrane-localized enhanced green fluorescent protein [GFP]) driven by myeloid-specific LysM-Cre mice (*mTmG f/f::LysM-Cre*). This system facilitated the visualization of myeloid lineage cells with a green label[26] (Figure S1). To observe the immune-vascular network during OIR, we utilized high-resolution two-photon microscopy on the intact OIR mouse retina (Figure S1A). Representative images displaying 3D reconstructions of retinal whole mounts in OIR mice at postnatal day (P) 17 are shown in Figure S1B. The location and morphology of myeloid lineage cells are depicted in Figures S1C and S1D. These findings illustrate the accumulation of myeloid cells during OIR. For a closer examination of the interaction between myeloid lineage cells and NV, we captured high-magnification confocal images of OIR retinas. These images revealed the recruitment of myeloid lineage cells to NV areas, as labeled by the endothelial cell marker CD31 (Figure S1E). Notably, these myeloid cells comprised $IBA1^+$ microglia and macrophages (Figure S1F). These data underscore the activation and accumulation of myeloid cells, including activated microglia and macrophages during OIR, hinting at a potential role for myeloid cells in shaping the OIR retinal phenotype.

Myeloid Socs3 deficiency-induced severe NV phenotype in OIR mice

In a previous study, we reported the accumulation of myeloid cells in laser-induced CNV areas in myeloid SOCS3 knockout (*Socs3 cKO*) mice.[26] Utilizing these myeloid *Socs3 cKO* mice as a model, we delved

2–4. The areas in white boxes were enlarged. (C) Representative flat mounts of Lectin (red)-stained OIR retinas from *Socs3* floxed controls (*Socs3 f/f*) mice and myeloid SOCS3 deficiency (*Socs3 cKO*) mice at P17. Scale bar, 500 μm. (D) Quantification of the percentages of NV and VO relative to the total retinal areas in (C) (n = 26–35 retinas). $^{**}p < 0.01$. (E) Representative fundus image of myeloid *Socs3 cKO* mice and *Socs3 f/f* mice under normal condition or during OIR at P90 and P180 (top). Retinal blood vessels on the fundus images were labeled with dark dashed lines (bottom). (F) Tortuosity index and integrated curvature were quantified using ImageJ (n = 6–8). $^{*}p < 0.05$; $^{***}p < 0.001$; $^{****}p < 0.0001$. n.s., no significance.

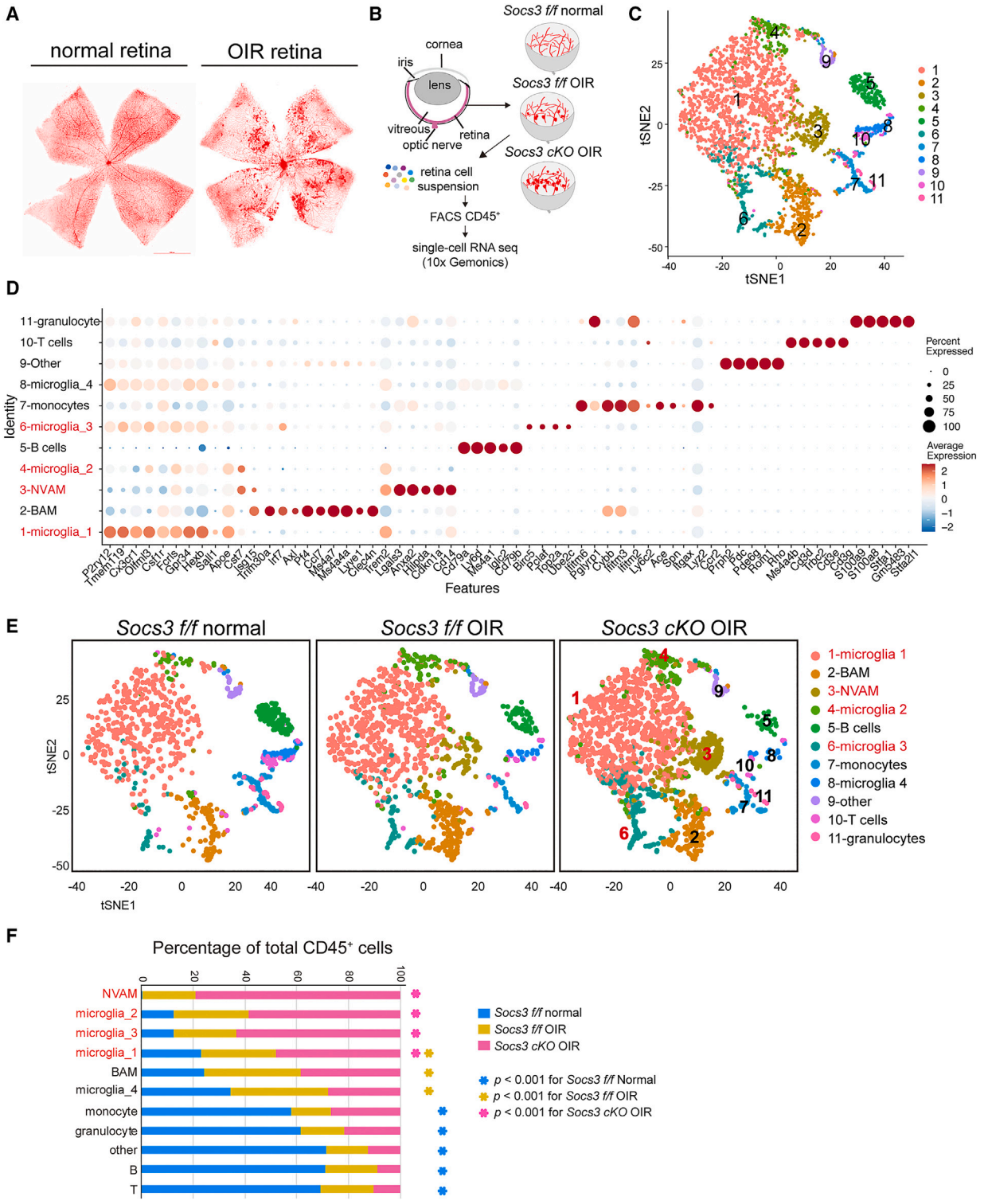

Figure 2. Characterization of immune cell types in retinas during OIR

(A) Schematic representation of retinal flat-mount images of normal and OIR retinas. (B) Workflow for 10x Genomics scRNA-seq on normal retinas (*Socs3 f/f* normal), OIR retinas (*Socs3 f/f* OIR), and myeloid SOCS3-deficient OIR retinas (*Socs3 cKO* OIR). (C) Identification of 11 distinct clusters of cells through single-cell transcriptomes of

(legend continued on next page)

into the molecular mechanisms through which myeloid cells regulate NV formation. Initially, we assessed the expression of SOCS3 in myeloid cells during OIR using myeloid-specific LysM-Cre-driven Ai9 tandem dimer Tomato (tdTomato) reporter mice (*Ai9 f/f::LysM-Cre*). These experiments revealed an upregulation of SOCS3 expression in myeloid cells, particularly in activated or amoeboid-shaped microglia and macrophages, in OIR retinas compared with normal retinas (Figure 1B).

Subsequently, we investigated the role of myeloid SOCS3 in pathological retinal angiogenesis by subjecting myeloid *Socs3 cKO* mice to OIR. *LysM-Cre* mice exhibited no abnormalities in retinal vasculature development at P7 and did not impact vaso-obliteration (VO) at P12 as well as NV and VO at P17 (Figures S2A and S2B). The deficiency of myeloid SOCS3 significantly augmented NV (Figures 1C and 1D), aligning with previous reports,[24] and exhibited no influence on retinal VO (Figure 1D) and body weights (Figure S2C). Furthermore, retinal vascular tortuosity was significantly exacerbated, as evidenced by an increased tortuosity index and integrated curvature, in myeloid *Socs3 cKO* OIR mice compared with control OIR mice (Figures 1E and 1F). In summary, these findings suggest that myeloid SOCS3 deficiency induces a severe NV phenotype and worsened vascular tortuosity in OIR mice.

Identification of distinct immune cell types in the mouse retina

To investigate the contribution of myeloid cells to NV development, scRNA-seq was performed on total immune cells isolated from normal retinas, OIR retinas, and retinas exhibiting a severe OIR phenotype in mice lacking myeloid SOCS3. Given that immune cells constitute approximately 1% of total retinal cells,[29] we enriched retinal immune cells by sorting them using CD45 antibodies for scRNA-seq (Figures 2A and 2B). The detailed information of scRNA-seq analysis, including cell number per group, mean reads per cell, and median genes per cell for the three groups, are provided in Table S1. The scRNA-seq data revealed 11 distinct clusters, as illustrated in t-distributed stochastic neighbor embedding (tSNE) plots (Figure 2C). These clusters were distinguished based on their unique expression of immune gene markers (Figure 2D), which were mapped to different immune cell types using the ImmGen ULI RNA-Seq database (Figure S3).

Among these 11 clusters, several expressed varying levels of microglial marker genes, such as *P2ry12*, *Tmem119*, *Cx3cr1*, *Olfml3*, *Csf1r*, *Gpr34*, and *Fcrl3*. Cluster 1, 4, 6, and 8 were identified as microglia 1, 2, 3, and 4, respectively, based on their marker gene expression profiles. Cluster 9, while displaying low levels of microglial markers, prominently expressed rod photoreceptor marker genes, including *Rho*, *Pde6g*, *Pdc*, *Prph2*, and *Rom1*, suggesting its potential identity as phagocytic microglia involved in the clearance of rod photoreceptor cell debris. However, further investigation is warranted to confirm this hypothesis, and cluster 9 was categorized as "other" cells.

Within the CNS, two major resident macrophage populations exist: microglia and border-associated macrophages (BAMs), also known as CNS-associated macrophages.[30] BAMs express specific genes such as *Pf4*, *Ms4a7*, and *Lyve1*, whereas microglia-specific markers like *P2ry12*, *Tmem119*, *Hexb*, and *Sall1* are not present in BAMs.[31] Thus, cluster 2 was identified as BAMs. Cluster 3 exhibited high expression of genes such as *Lgals3*, *Anxa2*, *Hilpda*, and *Cdkn1a*, coupled with downregulation of microglia markers (*P2ry12*, *Tmem119*, and *Cx3cr1*). *Trem2* and *Cst7* were also expressed in this cluster. Given its prevalence in OIR mice, not in normal mice, cluster 3 was identified as neovascular-associated microglia (NVAM).

Cluster 7, identified as monocytes, exhibited markers such as *Ccr2*, *Ly6c2*, *Ace*, *Spn*, *Ifitm2*, *Ifitm3*, *Ifitm6P*, *Glyrp1*, and *Cybb*. Cluster 11, classified as granulocytes, displayed marker genes including *S100a9*, *S100a8*, *Stfa1*, *Gm5483*, and *Stf2l1*. Additionally, two lymphoid lineage cell populations were detected. Cluster 5 was identified as B cells and displayed marker genes *Cd79a*, *Cd79b*, *Ly6d*, *Ms4a1*, and *Iglc2*. Cluster 10, representing T cells, was characterized by marker genes *Cd3d*, *Cd3e*, *Cd3g*, and *Trbc2*. All 11 distinct clusters of $CD45^+$ cells in the mouse retina at P13 in each group are illustrated in Figure 2E.

Accumulated microglia subsets during severe NV development

We next compared the proportion of cells in each cell cluster across the three groups—*Socs3 f/f* normal, *Socs3 f/f* OIR, and *Socs3 cKO* OIR—using a hypergeometric distribution test (Figure 2F). NVAM, microglia 1, microglia 2, and microglia 3 were significantly enriched in the *Socs3 cKO* OIR retinas. Microglia 1, BAM, and microglia 4 were significantly enriched in *Socs3 f/f* OIR retinas, but not in *Socs3 f/f* normal retinas. These data suggest that NVAM, microglia 1, microglia 2, and microglia 3 constituted a larger percentage of enriched immune cells in OIR retinas, potentially contributing to severe NV. To further investigate whether the functions of these microglia and macrophages are altered during OIR, we conducted Gene Ontology Biological Process (GOBP) analysis and Human Phenotype (HP) ontology analysis. Pathways linked to macrophage differentiation (Figure 3A), phagocytosis (Figure 3B), blood vessel endothelial cell proliferation involved in sprouting angiogenesis (Figure S4), blood vessel morphogenesis (Figure S4), and retinal NV (Figure S4) were all markedly enriched in both *Socs3 f/f* OIR retinas and *Socs3 cKO* OIR retinas compared with *Socs3 f/f* normal retinas, particularly in NVAM, microglia 1, 2, and 3. Additionally, pathways involved in cellular lipid metabolic processes, glucose metabolic processes, and lipid metabolic processes, enriched in $Spp1^+$ monocyte-derived macrophages in choroidal NV mice[32] and proliferative

immune cells from the three groups. (D) Expression of gene markers in the 11 identified cell clusters presented as the percentage expressed and average expression. BAM, border-associated macrophage; NVAM, neovascular-associated microglia. (E) Recapitulation of the 11 clusters identified across the three groups. (F) Proportion of cells derived from each group. *$p < 0.001$ by hypergeometric enrichment test. The color of asterisk indicates the enriched groups, and the names of significantly enriched cell clusters and the number of the clusters (#1, 3, 4, and 6) are labeled in red.

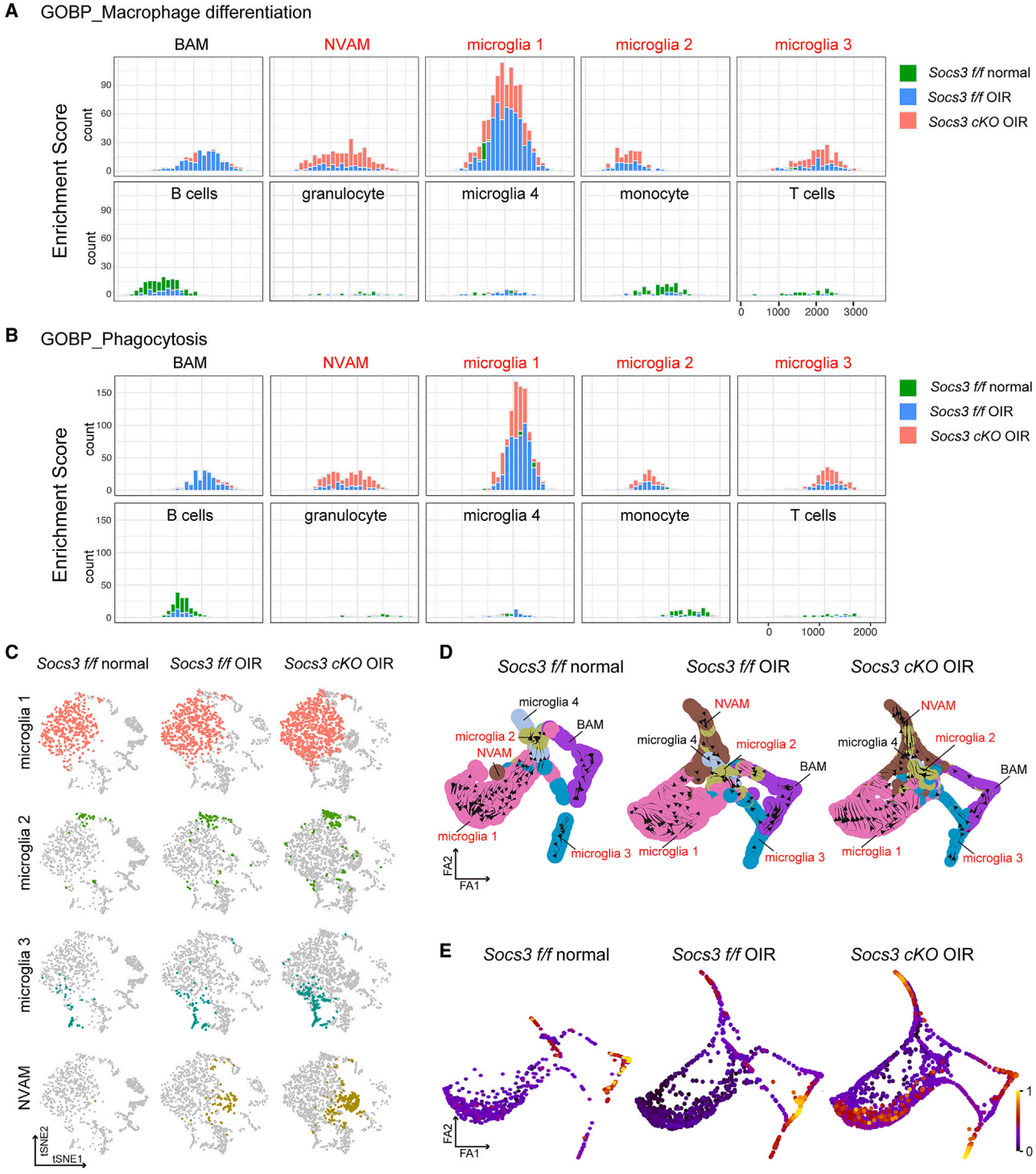

Figure 3. Accumulation of subsets of microglia clusters regulated by SOCS3 during OIR

(A) GOBP analysis depicting pathways involved in macrophage differentiation in the three groups. (B) GOBP analysis illustrating pathways involved in phagocytosis in the three groups. (C) tSNE plot showing the distribution of microglia 1, 2, 3, and NVAM within the total immune cells in the three groups. (D) RNA velocity analysis projected on ForceAtlas 2 (FA) embedding to represent cell fate transitions of significantly enriched clusters (microglia 1, 2, 3, and NVAM) in the three groups. (E) Pseudotime analysis of significantly enriched clusters (microglia 1, 2, 3, and NVAM) in the three groups, with latent time calculated using scVelo's latent time function. Early cell types (microglia 1) were assigned as early time points, while mature cells (BAM and NVAM) were associated with later time points.

retinopathy-associated microglia in OIR mice,[33] were also enriched in NVAM, microglia 1, 2, and 3 (Figure S4). The distribution of these four clusters is illustrated in Figure 3C. These findings strongly suggest that NVAM, microglia 1, 2, and 3 are closely associated with severe NV in OIR retinas. Notably, microglia 2, marked by high *Cst7* expression, was indicative of inflammatory microglia.[30] Microglia 3, which highly expressed *Pclaf* and *Top2a*, displayed characteristics suggestive of proliferative microglia.[34]

To gain insights into the developmental lineages and cellular dynamics of these microglia and macrophages during NV development, we conducted RNA velocity analysis on the scRNA-seq data and projected it onto the ForceAtlas 2 (FA) embedding (Figures 3D and S5A). This analysis was based on the relative abundance of nascent (unspliced) and mature (spliced) mRNA.[35] The trajectory of cell state transition and RNA velocities revealed a differentiation path (indicated as arrows) from microglia 1 (root microglia) to NVAM, both in *Socs3 f/f* OIR retinas and *Socs3 cKO* OIR retina (Figure 3D). The data suggest that NVAM is likely the most activated subset of microglia, especially in *Socs3 cKO* OIR retina. Additionally, while monocytes are known to differentiate into tissue macrophages, RNA velocity analysis for 11 clusters (Figure S5A) suggests that no cluster may originate from monocytes during OIR.

Furthermore, pseudotime analysis projected onto FA plots (Figure 3E) revealed that root microglia (microglia 1) in OIR retinas exhibit a more conservative, progenitor-like phenotype. Interestingly, the same cluster in *Socs3 cKO* OIR retinas included some transcriptionally different cells. NVAM displayed a longer pseudotime in OIR retinas and *Socs3 cKO* OIR retinas, suggesting its distinctiveness from the microglia root cluster (microglia 1) compared with other cells. Additionally, the population of BAM exhibited similarity to the root microglia in OIR, but it was much closer to NVAM in *Socs3 cKO* OIR retinas.

Collectively, these findings imply crucial roles for these microglia in retinal NV, contributing to the NV development through SOCS3 regulation.

SPP1-expressing microglia during ocular NV

To investigate the molecular mechanisms through which these microglia contribute to severe NV development, we conducted an analysis of differentially expressed genes (DEGs) in *Socs3 cKO* OIR retinas compared with *Socs3 f/f* OIR retinas using scRNA-seq data (Figure S5B). Among the top DEGs, *Spp1* stood out as the most highly upregulated DEG in various microglial subtypes, including microglia 1, 2, 3, and NVAM, indicating the potential role of *Spp1* in controlling microglia function during NV development. Furthermore, the expression of *Socs3* and *Spp1* in each cluster in the scRNA-seq dataset was analyzed (Figures S6A and S6B). In the OIR group (*Socs3 f/f* OIR), there was a notably higher population of *Socs3*-high cells (indicated by the black arrows in Figure S6A) compared with the normal group. Conversely, the *Socs3 cKO* OIR group exhibited a lower number of *Socs3*-high cells, confirming myeloid *Socs3* deficiency. It is worth noting that in the *Socs3 cKO* OIR group, there were still some cells expressing low levels of *Socs3* due to the limited efficacy of LysM-Cre recombination in retinal microglia.[36] Importantly, *Spp1*-expressing cells were predominately increased in subsets of microglia, particularly in the *Socs3 cKO* OIR retinas, as depicted by the FA plots (Figure 4A) and tSNE plots (Figures S6B and S6D). Notably, in the *Socs3 cKO* OIR retinas, there were more *Spp1*-expressing cells that exhibited low levels or lacked *Socs3* expression (Figures S6C and S6D).

Further examination of the localization of SPP1 expression in OIR retinas was performed on retinal cross-sections. These analyses revealed a robust induction of SPP1 in microglia and macrophages in OIR retinas compared with its weak expression under normal conditions. Importantly, SPP1 expression was further enhanced in the *Socs3 cKO* OIR retinas at P13, with a more substantial increase observed at P14 (Figure 4B). Of particular significance, SPP1 expression was localized in $IBA1^+$ cells exhibiting rounded shapes (Figure 4B, white box). Some $SPP1^+IBA1^-$ cells were also observed. The mRNA level of *Spp1* in $CD45^+$ cells isolated from retinas using magnetic-activated cell sorting with CD45 antibody was significantly higher in *Socs3 cKO* OIR retina at P13, with a further increase at P14 compared with control OIR retinas (Figure 4C).

We further evaluated the expression of *Spp1* in another angiogenesis mouse model, the laser-induced CNV model, which displays some aspects of NV similar to human neovascular AMD. Our prior research demonstrated that myeloid SOCS3 deficiency significantly increased laser-induced CNV.[26] Consequently, we assessed the expression of SPP1 in this laser-induced CNV mouse model. SPP1 expression was induced at day 1 post-laser exposure and continued to increase at day 3 post-laser exposure in this laser-induced CNV model (Figure S7A). Furthermore, SPP1 expression was notably upregulated in $IBA1^+$ cells surrounding the CNV lesion, particularly in *Socs3 cKO* mice at day 3 (Figure 4D). These findings suggest that $SPP1^+$ $IBA1^+$ microglia and macrophages may contribute to myeloid SOCS3 deficiency-induced retinal NV and laser-induced CNV development. Moreover, we assessed SPP1 expression in the CNV area in an eye from a patient diagnosed with nAMD. Elevated expression of SPP1, along with a greater presence of $SPP1^+IBA1^+$ double-positive microglia and macrophages, were discernible in the CNV area (indicated by a white dotted line based on DAPI staining) compared with the normal area within the same eye (Figure S7B), in line with previous observations.[28]

Next, we characterized these *Spp1*-expressing cells, particularly NVAM, using scRNA-seq data. We assessed the expression of classical microglia marker genes in these cells. Our findings indicated that during the transition from microglia 1 to NVAM, *Spp1* expression increased while the levels of *Cx3cr1* and *Tmem119* decreased (Figure S8). Subsequently, we determined the sources of SPP1 in retinas by performing CellChat analysis,[37] enabling the quantitative measurement of the SPP1 network within the immune cells in the database and predicting key incoming and outgoing signals of SPP1. This facilitated the interpretation of intercellular

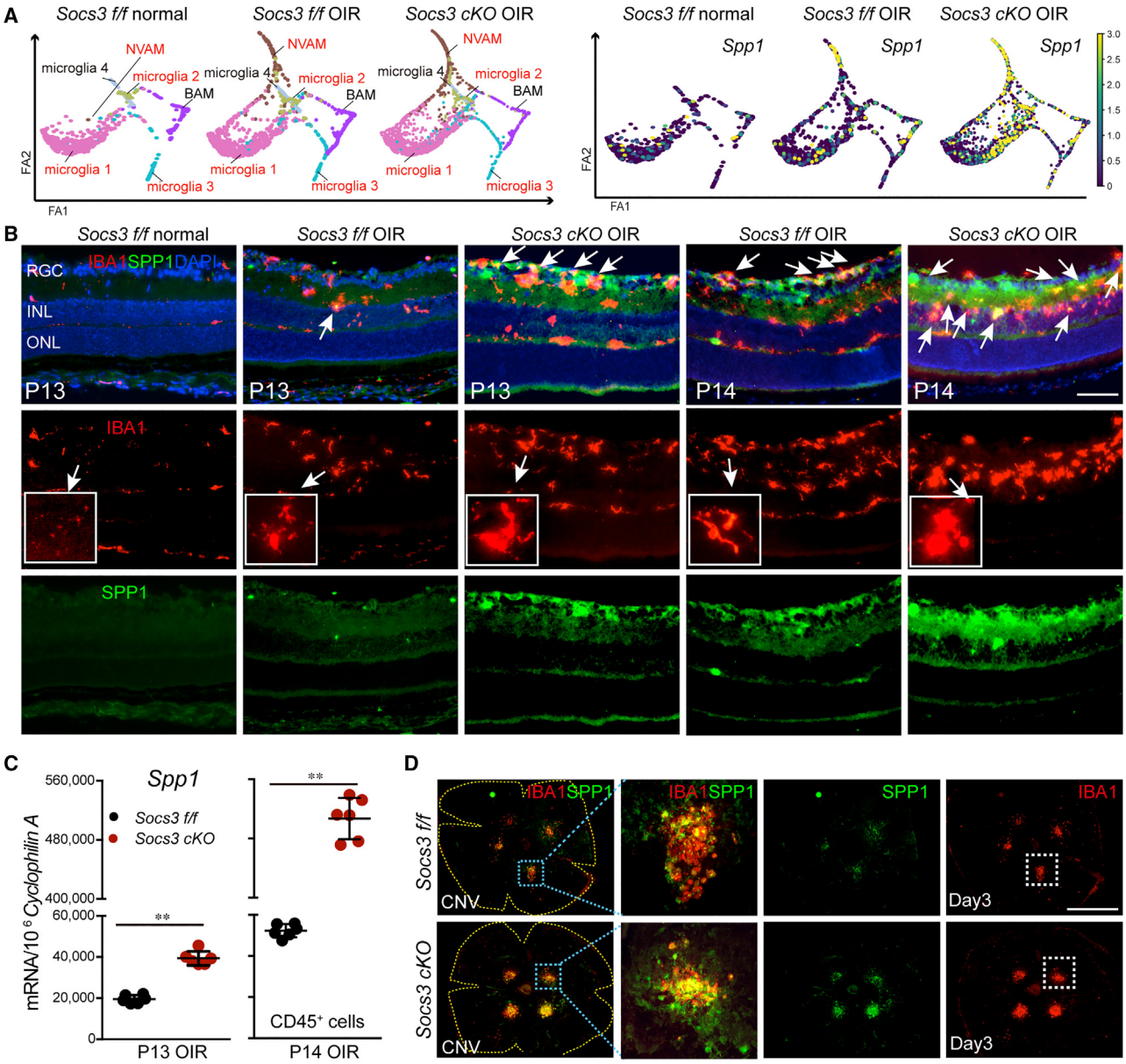

Figure 4. Induction of SPP1 in NVAMs in myeloid SOCS3-deficient OIR retinas

(A) ForceAtlas2 (FA) plots illustrating *Spp1* expressing in significantly enriched clusters across the three groups. (B) Representative cross-sections of IBA1 (red)- and SPP1 (green)-stained normal and OIR retinas from *Socs3 f/f* mice and *Socs3 cKO* mice at P13 and P14 (n = 6). DAPI (blue) indicates nuclei. White arrows in the top panel indicate SPP1$^+$ microglia, and the white boxes highlight enlarged round-shaped microglia. INL, inner nuclear layer; ONL, outer nuclear layer; RGC, retinal ganglion cell layer; Scale bar, 200 μm. (C) The mRNA expression of *Spp1* in CD45$^+$ cells isolated from *Socs3 f/f* and *Socs3 cKO* OIR mice at P13 and P14 (n = 6). **p < 0.01. (D) Representative flat mounts of IBA1 (red)- and SPP1 (green)-stained choroids from *Socs3 f/f* and *Socs3 cKO* mice with laser-induced CNV at day 3 post-laser (n = 6–8). The areas in the blue boxes indicating similar sizes of CNV lesions were enlarged. Scale bar, 500 μm.

communication involving SPP1 (Figure S9A). Under normal conditions, SPP1 was primarily released from BAM, microglia 1, and granulocytes among the immune cell types in our dataset. However, in OIR retinas, particularly in *Socs3 cKO* OIR retinas, NVAM emerged as the predominant source of SPP1, a cell type that was primarily found in *Socs3 cKO* OIR retinas but was scarcely present under normal conditions. Last, we predicted outgoing signaling from these cells and the top enriched pathways during NV using CellChat analysis. Our analysis revealed that more proangiogenic pathways, indicated by red arrows, including the VEGF pathway enriched in these cells, particularly, in NVAM from *Socs3 cKO* OIR retinas when compared with *Socs3 f/f* OIR retinas and *Socs3 f/f* normal retinas

(Figure S9B). The expression of the VEGF pathway including *Vegfa*, *Flt1*, and *Kdr* in each cell type was analyzed (Figure S9C), suggesting NVAM as a major immune cell source of *Vegfa* during severe NV development. Myeloid SOCS3 deficiency significantly induced the mRNA expression of *Vegfa* in choroidal/retinal tissues with CNV at day 3 post-laser (Figure S9D), which indicates the possibility of *Vegfa* induction in *Spp1*-expressing microglia and macrophages in myeloid SOCS3-deficient mice with severe NV.

Rescue of severe NV by deleting SPP1 in myeloid *Socs3*-deficient mice with OIR or CNV

To investigate the crucial role of SPP1 in NV development, particularly in the context of severe NV formation in myeloid *Socs3 cKO* OIR mice, we deleted the *Spp1* gene in myeloid *Socs3 cKO* mice by generating *Socs3 cKO* mice in a *Spp1* knockout (*Spp1 KO*) background (*Socs3 cKO::Spp1 KO*) and comparing them with *Socs3 f/f* mice in the *Spp1 KO* background (*Socs3 f/f::Spp1 KO*) (Figure 5A). Since variation in genetic background and body weights among different mouse strains can lead to variable severities of OIR,[38,39] we first examined retinal vascular development at P5 in normal mice and VO at P12 in OIR mice from *Spp1 KO*, *Spp1 Het*, and their littermate wild-type mice (Figures S10A–S10F), as well as *LysM-Cre* mice (Figure S2), and body weights under different conditions. No significant influences were observed. As shown in Figure 1C, myeloid SOCS3 deficiency in the *Spp1 WT* background significantly induced NV. Strikingly, deleting myeloid SOCS3 in the *Spp1 KO* background in *Socs3 cKO::Spp1 KO* OIR mice completely abolished the severe NV induced by myeloid SOCS3 deficiency. NV levels in these mice returned to levels in line with those in their littermate controls (*Socs3 f/f::Spp1 KO*) (Figures 5B and 5C). Their body weights were comparable at P17 in OIR (Figure S10G). This finding underscores the critical role of SPP1 in controlling the formation of retinal NV.

The critical control of SPP1 in NV formation was further evaluated in an additional angiogenesis mouse model, laser-induced choroidal NV mice. Myeloid SOCS3 deficiency had previously been showed to significantly increase laser-induced CNV[26] (Figures 5D and 5E). Remarkably, double knockout SPP1 and myeloid SOCS3 in *Socs3 cKO::Spp1 KO* mice abolished the severe NV induced by myeloid SOCS3 deficiency (Figures 5F and 5G). These results consistently demonstrated that SPP1 plays a critical role in controlling NV formation in both the retina NV model and the choroidal NV mouse model.

Direct regulation of SPP1 expression by STAT3

SOCS3 acts as a negative feedback regulator of the STAT3/interleukin-6 signaling pathway. We investigated whether STAT3 can directly regulate *Spp1* expression. To begin, we identified potential binding regions of STAT3 on the *Spp1* promoter and enhancer regions by analyzing chromatin immunoprecipitation sequencing (ChIP-seq) datasets of STAT3 (GSE86169)[40] and the ChIP-seq database of enhancer maker histone H3K27 acetylation (H3K27ac) (GSE188145).[41] Three potential regions (highlighted in red rectangle) containing the STAT3 consensus binding motif TTCNNNGAA[40,41] were identified and utilized for constructing luciferase reporters (Figure S11). Three reporters covered distinct regions: the promoter region (transcription start site [TSS] ~ -2.6 kb, containing four potential binding motifs) labeled as P2.6k, the enhancer region 1 (-6.5 kb ~ -7.0 kb, containing one potential binding motif) labeled as E1, and the enhancer region 2 (-7.5 kb ~ -9.0 kb, containing two potential binding motifs) labeled as E2 (Figure 6A).

We conducted a dual-luciferase reporter assay with these constructs, revealing that the promoter P2.6k was highly active, while the enhancers E1 and E2 showed low activity, indicating the potential binding of STAT3 to the region covering the *Spp1* promoter, not enhancers (Figure 6B). To confirm this binding, we transfected different doses of STAT3 into the dual-luciferase reporter assay, resulting in a dose-dependent increase in the reporter activity (Figure 6C). Furthermore, mutation of the four potential binding motifs attenuated the STAT3 dose-dependent response in luciferase reporter activity for the P2.6k construct (Figure 6C). This suggests that *Spp1* is a direct target of STAT3, which, in turn, is regulated by SOCS3.

The control of SPP1 by SOCS3/STAT3 was validated *in vivo* using a laser-induced CNV model (Figures 6D–6F). In myeloid SOCS3-deficient Ai9 reporter mice with laser-induced CNV, the area containing tdTomato$^+$ SPP1$^+$ cells around CNV increased compared with control mice (Cre along reporter mice) (Figure 6D). Moreover, the cell number of tdTomato$^+$ SPP1$^+$ cells in retinas from myeloid SOCS3-deficient reporter CNV mice was substantially higher compared with control mice (Figure 6E). Additionally, SOCS3 provides negative feedback to STAT1, to a lesser extent than STAT3.[42] An increased level of phosphorylated STAT1, indicating STAT1 activation, was also observed in CNV lesion areas in myeloid SOCS3-deficient Ai9 reporter mice compared with control mice (Figure S12). Importantly, tdTomato$^+$ SPP1$^+$ cells were positive for phospho-STAT3, indicating STAT3 activation (Figure 6F). These results confirmed the direct role of STAT3 in regulating SPP1 expression during NV development.

Inhibition of NV in OIR through targeting the SOCS3/SPP1 pathway

We explored the potential of targeting the SOCS3/SPP1 pathway to inhibit NV in OIR. First, we generated SOCS3 overexpression mice (*Socs3* cOE) driven by LysM-Cre. Both *Socs3 OE floxed* mice and *Socs3 cOE* mice do not display any abnormalities in normal retinal vasculature and body weights (Figures S13A–S13C). Remarkably, the overexpression of SOCS3 significantly suppressed retinal NV while leaving retinal VO unaffected (Figures 7A and 7B). This further underscores the crucial role of SOCS3 in directly influencing retinal NV development. We then explored the effects of interventions with potential therapeutic agents. Naringenin has been reported to induce SOCS3[43,44] and treatment with naringenin from P12 to P16 results in a significant reduction in NV by about 50% at P17 compared with controls (Figures 7C and 7D). An SOCS3 mimetic peptide, named as KIRESS,[45] which incorporates the KIR and ESS regions of SOCS3, exhibits the ability to bind to JAK2. In a previous

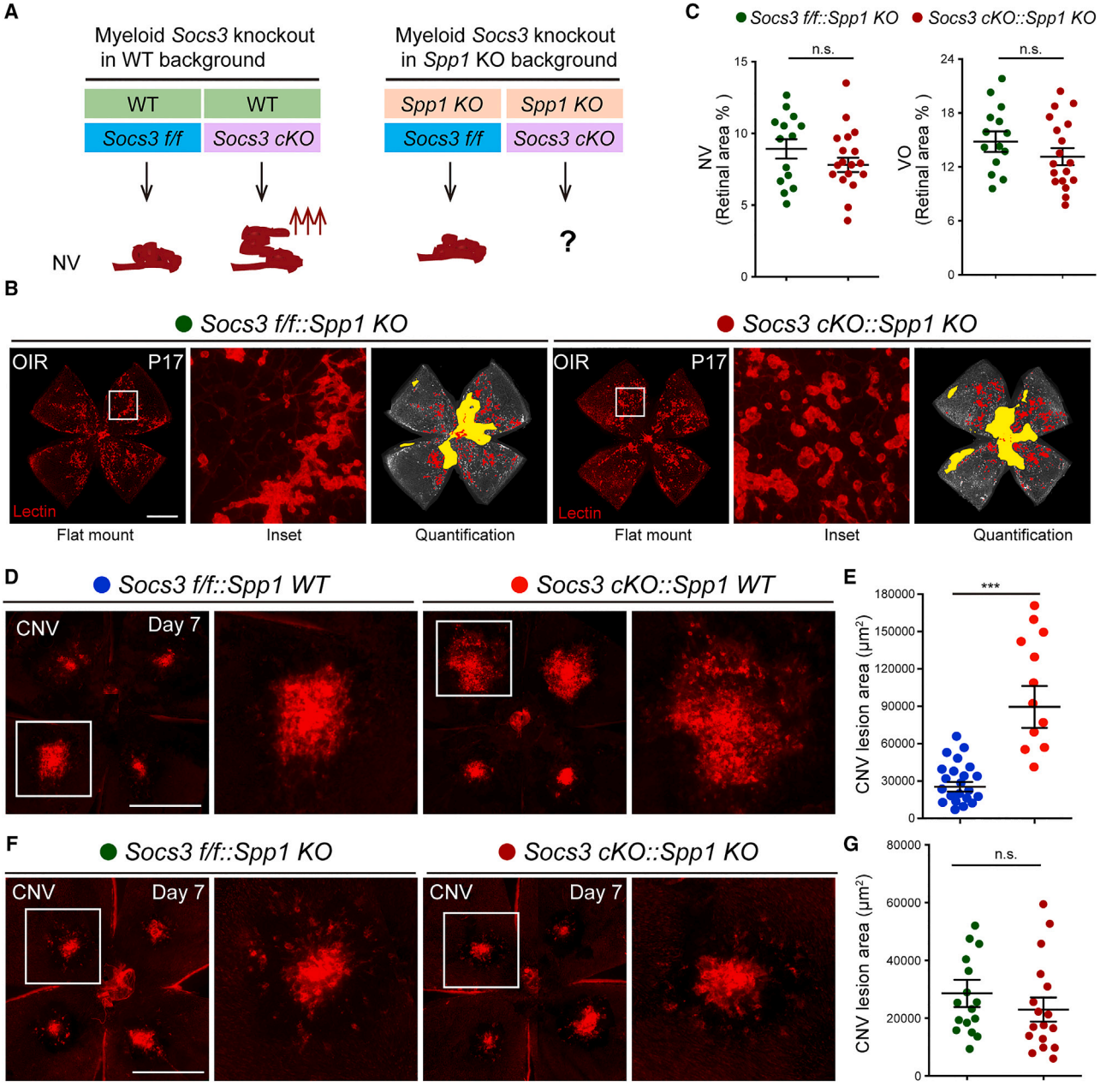

Figure 5. Suppression of myeloid *Socs3* deficiency-induced NV by *Spp1* inhibited in two angiogenesis mouse models

(A) A schematic illustrating the strategy of deleting myeloid SOCS3 in wild-type (WT) genetic background or a *Spp1* knockout background. (B) Representative retinal flat mounts of Lectin (red)-stained OIR retinas from myeloid SOCS3 knockout mice in *Spp1* knockout background (*Socs3 cKO::Spp1 KO*) and *Socs3* floxed mice in *Spp1*knockout background *(Socs3 f/f:: Spp1 KO)* at P17. NV areas in the white boxes (inset panel) were enlarged. In the Quantification panel, red areas indicate NV and yellow areas indicate VO. Scale bar, 1,000 μm. (C) Quantification of the percentages of NV and VO relative to the total retinal areas in (B) (n = 14–18 retinas). (D) Representative flat mounts of Lectin-stained choroids from myeloid SOCS3 knockout mice in WT background (*Socs3 cKO::Spp1 WT*) and *Socs3* floxed mice in WT background *(Socs3 f/f:: Spp1 WT)* with laser-induced CNV at day 7 post-laser. The CNV areas in the white boxes were enlarged. Scale bar, 500 μm. (E) Quantification of CNV lesion areas in each group in (D) (n = 12–20 retinas). ***p < 0.001. (F) Representative Lectin (red)-stained choroidal flat mounts from myeloid SOCS3 knockout mice in *Spp1 KO* background (*Socs3 cKO::Spp1 KO)* and *Socs3* floxed mice in *Spp1* knockout background *(Socs3 f/f:: Spp1 KO)* with laser-induced CNV at day 7 post-laser. The CNV areas in the white boxes were enlarged. Scale bar, 500 μm. (G) Quantification of CNV lesion areas in each group in (F) (n = 16–17). n.s., no significance.

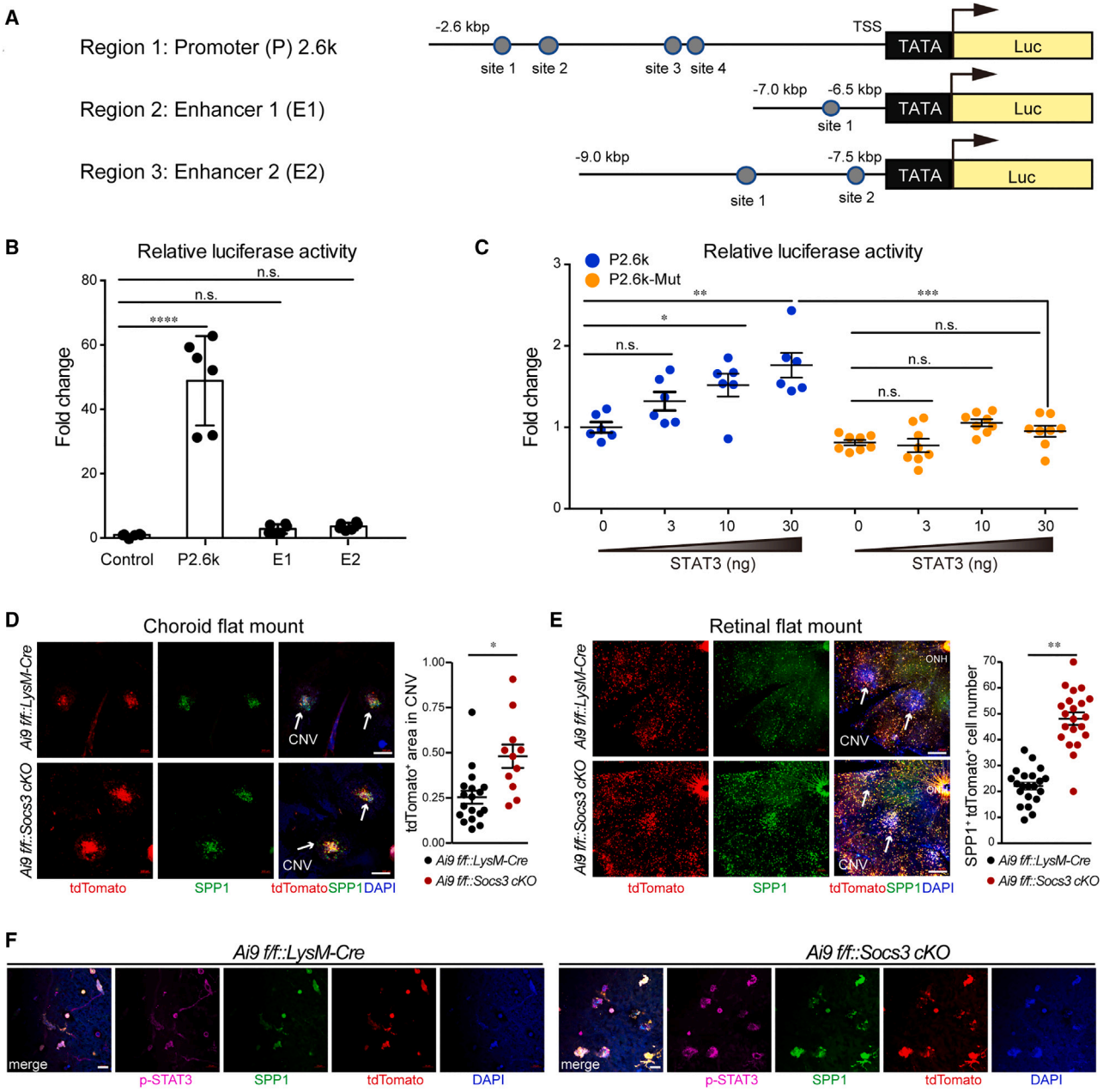

Figure 6. *Spp1* as a direct target of STAT3

(A) Schematic representation of three luciferase reporters, including the *Spp1* promoter (P2.6k), enhancer region 1 (E1), and enhancer region 2 (E2). Three 5′ regions of the *Spp1* gene were subcloned into the luciferase reporter pTA-luc plasmid. The gray dots indicate putative STAT3 binding sites. Luc, luciferase; TATA, a TATA box. (B) Fold changes in relative luciferase activities (normalized with Renilla luciferase activities) for P2.6k, E1, and E2 vs. the control (empty pTA-luc vector) (n = 6). ****p < 0.0001; n.s., no significance. (C) Fold changes in relative luciferase activities (normalized with Renilla luciferase activities) for P2.6k and P2.6k-mutant (P2.6k-Mut) co-transfected with a STAT3-expressing vector (n = 6–8). P2.6k-Mut: STAT3 binding sites in P2.6k were mutated from TTCNNNGAA to GTGNNNCAC. *p < 0.05; **p < 0.01; ****p < 0.0001; n.s., no significance. (D) Representative choroidal flat mounts from *Ai9 f/f::Socs3 cKO* and *Ai9 f/f::LysM-Cre* mice with laser-induced CNV at day 3 post-laser and quantification of tdTomato$^+$SPP1$^+$ areas in CNV (n = 12–19). Scale bar, 200 μm. (E) Representative retinal flat mounts from *Ai9 f/f::Socs3 cKO* and *Ai9 f/f::LysM-Cre* mice with laser-induced CNV at day 3 post-laser and quantification of tdTomato$^+$SPP1$^+$ cell numbers in retinas (n = 21–23). Scale bar, 200 μm. (F) Representative flat mounts of SPP1 (green)- and phospho-STAT3 (magenta)-stained retinas from *Ai9 f/f::Socs3 cKO* and *Ai9 f/f::LysM-Cre* tdTomato (red) reporter mice with laser-induced CNV at day 3 post-laser. DAPI (blue) indicates nuclei. Scale bar, 20 μm.

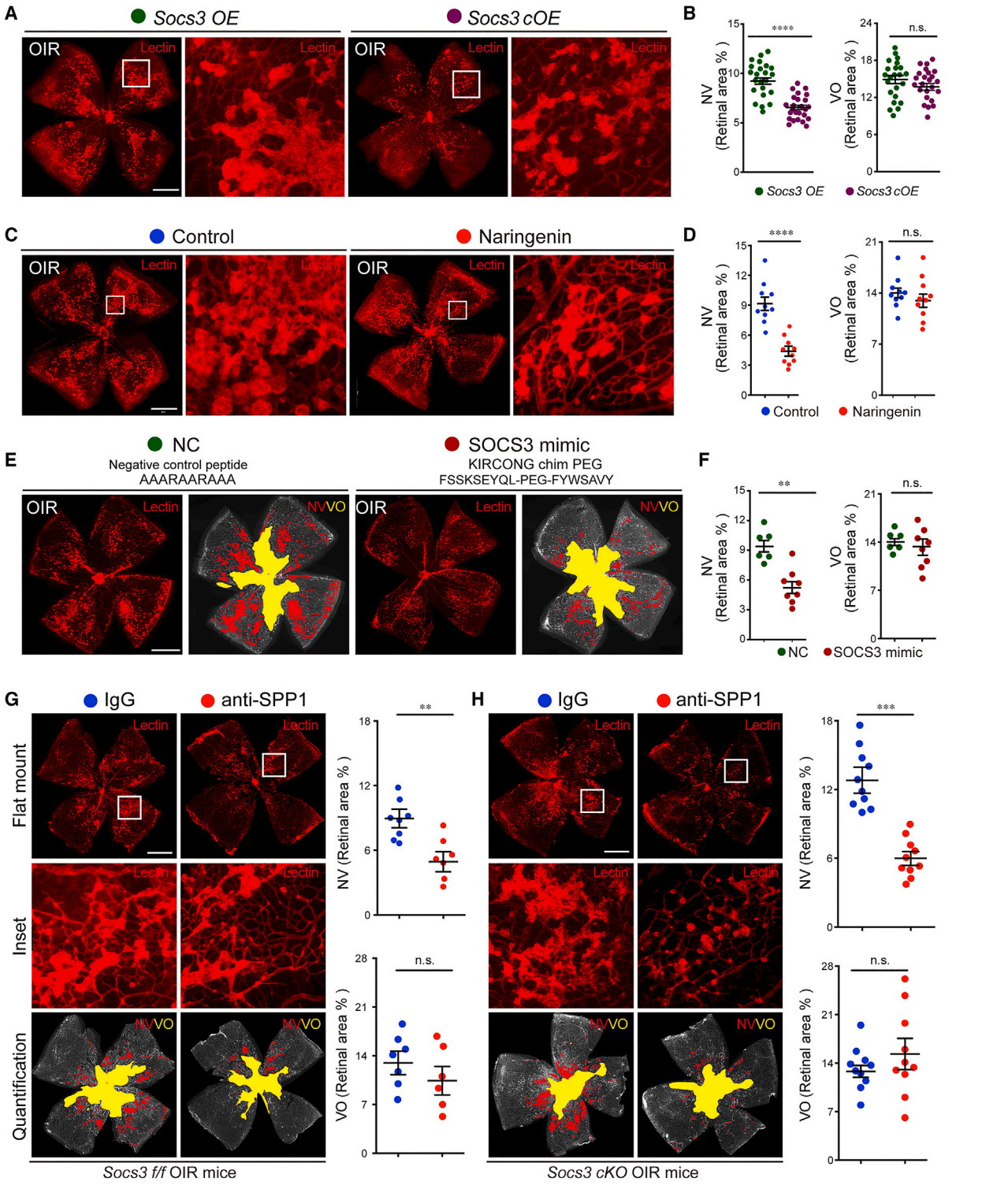

Figure 7. Inhibition of NV in OIR retinas by induction of SOCS3 or blocking SPP1

(A) Representative Lectin (red)-stained retinal flat mounts from myeloid SOCS3 overexpression (*Socs3 cOE*) OIR mice and littermate *Socs3* floxed controls (*Socs3 OE*) OIR mice. Scale bar, 1,000 μm. (B) Quantification of the percentages of NV and VO relative to the total retinal areas in (A) (n = 23–25 retinas). ****p < 0.0001, n.s., no significance. (C) Representative Lectin (red)-stained retinal flat mounts from OIR mice naringenin- or control-intraperitoneally injected from P12 to P16. Scale bar, 1,000 μm. (D)

(legend continued on next page)

study,[26] we demonstrated the efficacy of this peptide in suppressing laser-induced CNV with a relative lower efficacy than naringenin and SOCS3 genetic overexpression due to limited water solubility. Another mimetic of SOCS3, named KIRCONG chim,[46] is a chimeric peptidomimetic constituted by two non-contiguous protein fragments, KIR and CONG, held together by non-native β-Alanines. This proteomimetic demonstrated ability to mimic SOCS3 biology in vascular smooth muscle cells (VSMCs),[46] but also presented a limited water solubility to induce the design of analogues.[47] KIRCONG chim PEG is a SOCS3 mimetic peptide that is analogous to previous mimetics of SOCS3 deriving from a protein dissection approach and contains a polyethylene glycol (PEG) moiety as spacer instead of the two β-Alanines of KIRCONG chim. Our data demonstrated that KIRCONG chim PEG treatment administrated from P12 to P16, significantly suppressed NV by about 40% at P17 (Figures 7E and 7F). Furthermore, we explored the efficacy of SPP1 neutralizing antibody treatment in OIR mice through intravitreal injection at P14. This intervention reduced NV by 41% in *Socs3 f/f* OIR mice (Figure 7G) and by 67% in *Socs3 cKO* OIR mice (Figure 7H) at P17 compared with control immunoglobulin (Ig)G treatment. None of the above treatments had any discernible impact on mouse body weights (Figure S13D). Notably, SPP1 neutralizing antibody treatment reduced laser-induced CNV by 64.3% in *Socs3 f/f* OIR mice (Figures S14A and S14B) and by 70% in *Socs3 cKO* mice (Figures S14C and S14D) at day 7 post-laser compared with control IgG treatment. These results suggest that targeting the SOCS3/SPP1 pathway holds promise as a therapeutic strategy for inhibiting pathological NV in retinal diseases.

DISCUSSION

In this study, we initially observed the accumulation of SPP1-expressing microglia and macrophages during the formation of retinal NV and CNV. Second, we demonstrated that deleting SPP1 effectively rescued severe NV induced by myeloid SOCS3 deficiency in both OIR and CNV mouse models. Third, we identified a central regulatory pathway, SOCS3/STAT3/SPP1, responsible for controlling the function of SPP1-expressing microglia during the development of NV. Furthermore, we explored the therapeutic potential of targeting the SOCS3/SPP1 pathway. Activation of SOCS3 with mimetic peptides and small molecules (such as naringenin), or inhibition of SPP1 with neutralizing antibodies demonstrated promising outcomes for treating ocular NV. Overall, our findings provide a comprehensive understanding of the critical role of SPP1-expressing microglia and macrophages and the SOCS3/STAT3/SPP1 pathway in pathological angiogenesis in the context of myeloid SOCS3 deficiency. These discoveries may pave the way for therapeutic approaches to manage ocular NV effectively.

Previous scRNA-seq studies[48] have identified various cell types involved in retinopathies using OIR mice. Microglia, as the principal resident immune cells in the retina,[49,50] are intimately linked to retinal angiogenesis.[51,52] A prior study on scRNA-seq analysis of $CD11b^+$ myeloid lineage cells in OIR retinas identified a subpopulation of microglia exhibiting elevated expression of necroptosis-related genes *Rip3* and *Mlkl*, suggesting a potential therapeutic approach by targeting microglia for retinal neovascular diseases including ROP.[53] Meanwhile, another study of scRNA-seq on $CD11b^+$ $F4/80^+$ microglia/monocytes/macrophages in OIR retinas reveals several types of microglia associated with proliferative retinopathy, such as microglia subsets characterized by high self-renewal capacities and a hypermetabolic microglia subset.[33] These prior findings underscore the pivotal roles of microglia in the development of ROP. It is important to note that ROP manifests in varying degrees, and not all cases lead to blindness. While some infants experience mild ROP and naturally recover without intervention, others face severe ROP requiring treatment to avert blindness. A comprehensive understanding of the mechanisms underpinning severe ROP is crucial for improving the prognosis and outcomes of affected infants. In this context, the study conducted by Xu's group elucidated that the absence of myeloid SOCS3 exacerbates NV during OIR.[24] Our data corroborated these findings by demonstrating that myeloid SOCS3 deletion significantly elevated retinal NV and exacerbated tortuosity of posterior retinal vessels in OIR retinas. It is worth noting that retinal vascular tortuosity is closely associated with severe forms of ROP[54] and represents a hallmark of ROP plus disease, characterized by the most severe vascular alterations, including dilation and tortuosity.[55] To investigate the role of myeloid lineage cells during the pathogenesis of severe ROP, we utilized *Socs3 cKO* OIR mice as a model with severe NV. Our scRNA-seq data analysis unveiled an increase in the relative abundance of distinct subpopulations of microglia in *Socs3 cKO* OIR retinas, aligning with the observed escalation in NV and the activation of pathways associated with macrophage differentiation and phagocytosis. Consequently, we associated this unique population of SPP1-expressing microglia with the heightened NV in this severe NV model. Notably, a parallel can be drawn between the newly identified SPP1-expressing microglia and a subset of disease-associated microglia (DAM) discovered in brain lesions associated with conditions like Alzheimer's disease (AD), amyotrophic lateral sclerosis, and aging.[56,57] The gene signature of cluster 3, namely NVAM, resembles that of DAMs in the context of AD.[56,57] These immune cells express classic microglial markers (*Iba1*, *Cst3*, and *Hexb*) alongside the downregulation of "homeostatic" microglia genes (*P2ry12*, *Cx3cr1*, and *Tmem119).* Furthermore, there is an upregulation of genes linked to lysosomal phagocytic and lipid metabolism pathways (*Apoe*, *Lpl*, and *Trem2*). This indicates that NVAM may be actively

Quantification of the percentages of NV and VO relative to the total retinal areas in (C) (n = 10 retinas). ****p < 0.0001, n.s., no significance. (E) Representative Lectin (red)-stained retinal flat mounts from OIR mice intravitreally injected with SOCS3 peptide mimic (KIRCONG chim PEG) or control peptide at P12. Scale bar, 1,000 μm. Red, Lectin, or NV area; yellow, VO area. (F) Quantification of the percentages of NV and VO relative to the total retinal areas at P17 in (E) (n = 8). **p < 0.01, n.s., no significance. (G) Representative Lectin (red)-stained retinal flat mounts from *Socs3 f/f* OIR mice and *Socs3 cKO* OIR mice OIR mice intravitreally injected with SPP1 neutralizing antibody or control antibody at P14. Scale bar, 1,000 μm. Red, Lectin, or NV area; yellow, VO area. (H) Quantification of the percentages of NV and VO relative to the total retinal areas at P17 (n = 6–9). **p < 0.01; ***p < 0.001, n.s., no significance.

involved in the pathogenesis of severe ROP. However, a recent study has highlighted phenotypic heterogeneity within the DAM population in the context of aging and neurodegeneration.[58] The DAM population can be divided into two distinct cell lineages: DAM and monocyte-derived disease inflammatory macrophages (DIM). Although both populations exhibit high expression of *Trem2*, they differ in other gene markers. Specifically, DAMs show relatively lower expression of *P2ry12* and *Cx3cr1* compared with DIMs, along with higher expression of *Itgax/Cd11c*. In our study, we observed lower expression of *P2ry12* and *Cx3cr1* in cluster 3, along with very low expression of *Itgax*, suggesting the similarity of cluster 3 with DAM. Furthermore, our analysis revealed that DIMs-conserved genes,[58] including *Ctss*, *Il1b*, and *Cd14*, were listed in the top 20 DEGs (Figure S5B) or highly expressed (Figure 2D) in cluster 3. These findings suggest that cluster 3 harbors a mixed gene signature of both DAM and DIM. Additionally, $SPP1^{+}$ monocyte-derived macrophages (MDMs) were identified in experimental CNV mice[32,59] and these MDMs displayed increased expression of *Vegfa*, *Lgals3*, *Fn1*, and *Anxa2*, as well as *Itgax*. These gene signatures were also found in cluster 3. These findings indicate a gene signature of DAM, DIM, or MDMs in cluster 3. Due to the analysis of a small population of cells in our study, we did not observe distinct subpopulations in cluster 3. These cells associated with NV development in cluster 3 might encompass DAMs, DIMs, and even MDMs, requiring further investigation for precise determination.

SPP1 is expressed not only in myeloid lineage cells but also by multiple cell types in mouse retinas, exhibiting distinct patterns across various physiological and pathological conditions. For instance, it is expressed in alpha retinal ganglion cells[60] and optic nerve astrocytes following injury.[61] To ascertain that the severe NV development in *Socs3 cKO* OIR retinas can be attributed specifically to SPP1 from myeloid cells, we compared the extent of NV in *Socs3 cKO* OIR retinas to *Socs3 f/f* OIR retinas with equivalent SPP1 levels, achieved by introducing the *Spp1* knockout background. Importantly, the heightened NV resulting from myeloid deficiency in wild-type background did not manifest in *Socs3 cKO* OIR retinas with the *Spp1 KO* background. Hence, the significant increase in NV observed in *Socs3 cKO* OIR mice was regulated by *Spp1*. Alternatively, the use of *Spp1* floxed mice[61] offers the possibility of specifically knocking out *Spp1* in myeloid cells through breeding with *Socs3 cKO* driven by LysM-Cre or Cx3cr1-Cre, presenting a valuable avenue for future investigations.

SOCS3/SPP1 may exert control over NV in OIR retinas through indirect mechanisms, such as the modulation of SPP1-expressing microglia function to influence other proangiogenic factors, notably the VEGF pathway. Alternatively, these pathways may have a direct impact on endothelial cell growth, as previously reported,[62,63] through activation of the endothelial Kit/Akt/mTOR pathway.[63]

Our prior research has unveiled the ability of neuronal and glial SOCS3 to suppress pathological retinal angiogenesis in OIR mice by VEGFA.[22] In this study, we also noticed that the VEGF pathway was highly enriched in myeloid SOCS3-deficient OIR mice. We further examined this in CNV mice, and our data showed that the mRNA expression of *Vegfa* in choroid/retina complexes from *Socs3 cKO* CNV mice was significantly higher than in *Socs3f/f* control CNV mice, suggesting that SOCS3 regulates *Vegfa* in myeloid cells during NV. Based on our CellChat data (Figure S9B), *Spp1* was highly enriched in NVAM in both *Socs3 f/f* OIR and *Socs3 cKO* OIR mice, but the VEGF pathway was highly enriched in NVAM only in *Socs3 cKO* OIR mice, suggesting that myeloid SOCS3 may determine the enrichment of the VEGF pathway in NVAM during OIR. Myeloid SOCS3 deletion promoted the enrichment of both the VEGF and SPP1 pathways in NVAM during OIR. Whether SPP1 has any effect on the transcription of VEGF or any other pro-angiogenic effectors, and whether and how VEGFA and SPP1 can work synergistically during NV remain unclear.

The *Spp1* locus has been found to undergo regulation by multiple transcriptional factors in various disease contexts. For instance, studies have reported the binding of c-Myc and OCT-1 to the proximal promoter of the *Spp1* gene in U251MG and U87MG human glioma cells.[64] In colorectal cancer cells, transcription factors ETS-1 and RUNX2 have been identified as regulators of *Spp1* expression.[65] In melanoma cells, transcription factors c-Myb,[66] AML-1a, and C/EBPα were found to bind to the *Spp1* gene promoter.[67] In our study, we have identified a direct transcriptional regulation of *Spp1* by STAT3 in the retinas. Nevertheless, it remains a subject of further exploration whether *Spp1* is concurrently controlled by other transcriptional factors in these mice, such as HIF1α.[68] Additional investigations are required to shed light on potential synergistic regulation involving multiple transcription factors.

In our study, we have underscored the significant translational potential of targeting the SOCS3/SPP1 pathway for the treatment of vascular eye diseases, like AMD and ROP. Naringenin can induce SOCS3[43,44] and its efficacy in markedly suppressing laser-induced CNV has been demonstrated in our previous work.[26] Here our results support this by revealing that naringenin reduces retinal NV. Moreover, we delved into the effects of a chimeric water-soluble SOCS3 mimetic, KIRCONG chim PEG,[47] in the OIR mouse model. KIRCONG chim PEG, featuring a polyethylene glycol (PEG) moiety as a spacer instead of the two β-Alanine molecules of KIRCONG chim, impressively suppressed NV. Furthermore, we demonstrated the therapeutic potential of SPP1 neutralizing antibodies administrated via intravitreal injection, effectively preventing NV in myeloid SOCS3 deficient OIR mice. This underscores the translational promise of targeting SPP1 in the context of severe NV. In line with our findings, Beguier et al. reported robust induction of SPP1 by high-temperature requirement A serine peptidase 1 (HTRA1), a factor strongly elevated in AMD retinas. The study showed that HTRA1-induced increase in CNV formation was significantly mitigated by SPP1 neutralizing antibody treatment,[69] highlighting the therapeutic prospects of SPP1 inhibitors for AMD treatment. Notably, the impact on NV development in two models (OIR and CNV) differed in *Spp1 KO* mice or with anti-SPP1 treatment,[28,69,70] suggesting that systemic application and local intravitreal injection of anti-SPP1 may exert

varying effects on NV development.[28] The precise underlying mechanisms warrant further investigation.

It is crucial to acknowledge that the utilization of LysM-Cre in this study to manipulate the expression of SOCS3 in myeloid cells introduces a potential limitation in thoroughly investigating the various populations and origins of NVAM, DAM, DIM, or MAM during NV. Our data analysis revealed a notable observation in OIR retinas from myeloid SOCS3-deficient mice driven by LysM-Cre, where some cells were found to express low levels of *Socs3*. This occurrence is primarily attributed to the documented low efficacy of LysM-Cre recombination in retinal microglia,[36] which primarily targets monocytes and neutrophils.[71] Therefore, while our study provides valuable insights into the impact of SOCS3 deficiency in myeloid cells during NV, it is imperative to interpret our results within the context of the limitations related to the specificity and efficiency of LysM-Cre recombination in retinal microglia. Future investigations employing alternative or complementary approaches to manipulate SOCS3 expression in a more cell-type-specific manner may be warranted to further elucidate the intricate cellular dynamics of microglia involved in NV processes in the retina.

Our findings establish that SPP1 plays a pivotal role in determining pathological retinal blood vessel growth in vascular eye diseases. Moreover, we elucidated the crucial role of the SOCS3/STAT3/SPP1 pathway in governing the accumulation of SPP1-expressing microglia and macrophages during the development of pathological ocular NV. Targeting SPP1-expressing microglia and macrophages via the SOCS3/STAT3/SPP1 pathway represents a promising approach to potentially treat ocular neovascularization.

MATERIALS AND METHODS

Animals

All animal studies were approved by the Boston Children's Hospital Institutional Animal Care and Use Committee. The ethical use of animals was according to the guidance of The Association for Research in Vision and Ophthalmology. Both male and female mice were included in the experiments and randomly grouped. Age-matched flox/flox mice, Cre mice, or wild-type mice were used as controls. The floxed *Socs3 (Socs3 f/f)* mouse line was generously provided by Dr. A. Yoshimura.[72] The floxed mouse line for *Socs3* overexpression *(Socs3 OE)* was a gift from Dr. Allison W. Xu.[73] LysM-Cre mice (stock# 004781), C57BL/6J mice (stock# 000664), mTmG reporter mice (stock# 007576), Ai9 reporter mice (stock# 007909), and *Spp1* knockout mice (stock# 004936) were obtained from the Jackson Laboratory. Littermate or age-matched floxed mice, Cre mice, and wild-type mice were used as controls.

Oxygen-induced retinopathy mouse model

The oxygen-induced retinopathy (OIR) model was achieved using neonatal mice as described previously.[25] Briefly, mouse pups with nursing female mice were exposed to 75% oxygen from postnatal day (P) 7 to P12, then returned to room air until P17 for phenotypical analysis and gene expression analysis at indicated times. For phenotypical analysis, retinas were collected at P17, dissected, stained overnight with fluorescent dye conjugated Griffonia Simplicifolia Isolectin B_4 (Invitrogen, I21413), and flat-mounted. The avascular (vaso-obliteration [VO]) and pathological NV areas were quantified[74] by masked researchers using ImageJ (National Institutes of Health) or fully automated deep learning segmentation method.[75] The exclusion criteria for the OIR mouse model were used as previously described.[76]

Immunostaining, confocal imaging, and two-photon microscopy imaging

Mouse eyes were isolated and fixed with 4% paraformaldehyde (PFA) at room temperature for 1 h. Following fixation, the eyes were washed with 0.01 M phosphate buffered saline (PBS) three times. Retinas were dissected from the fixed eyes, embedded, sectioned, and permeabilized using 0.01 M PBS with 0.3% Triton X-100. The flat-mounted retinas or cross-sections were stained with antibodies according to the manufacturer's instructions and imaged using a confocal microscope (Zeiss LSM700 and LSM980). For two-photon imaging, mTmG reporter mice were intravenously injected with Qtracker655-CD31 antibody before being euthanized. Retinas were dissected without fixation and mounted for imaging. The following primary antibodies were used: SPP1 (R&D Systems, AF808, RRID: AB_2194992), IBA1 (Wako, 019–19741, RRID: AB_839504), Isolectin B4 (ThermoFisher Scientific, I21411, RRID: AB_23146), CD31 (MEC 13 · 3, BD Biosciences, 550274, RRID: AB_393571), SOCS3 (abcam, ab16030, RRID:AB_443287), PE anti-mouse/human CD11b (BioLegend, 101207, RRID:AB_312790), and GFP (Abcam, ab13970, RRID: AB_300798); and the following secondary antibodies were used: Goat anti-Rabbit IgG, Alexa Fluor 594 (ThermoFisher, A-11037, RRID:AB_2534095), Goat anti-Rabbit IgG, Alexa Fluor 488 (ThermoFisher, A-11008, RRID:AB_143165), Goat anti-Chicken IgY, FITC (ThermoFisher, A16055, RRID:AB_2534728), Goat anti-Mouse IgG, IgM, IgA (H + L), Alexa Fluor 488 (ThermoFisher, A-10667, RRID:AB_2534057), Goat anti-Mouse IgG, Alexa Fluor 594 (ThermoFisher, A-11005, RRID:AB_141372), Donkey anti-Rabbit, Alexa Fluor 647 (ThermoFisher, A-31573, RRID:AB_2536183), Donkey anti-Goat IgG, Alexa Fluor 647 (ThermoFisher, A-21447, RRID:AB_141844), and DAPI (Vector Labs, H-1200-10).

Mouse fundus imaging and retinal vessel tortuosity quantification

Mice were anesthetized by intraperitoneal injection of a ketamine and xylazine mixture. Tropicamide solution (1%) (Akorn, NDC 17478-102-12) was applied to the eyes of anesthetized mice to dilate the pupils. Eyes were rinsed with artificial tears (K.C. Pharmaceuticals, NDC 55651-03) to remove tropicamide before imaging. Fluorescein sodium salt (Sigma, F6377) was intraperitoneally injected. The eyes of the anesthetized mice were positioned for fundus imaging using the Retinal Imaging System (Micron IV, Phoenix). The eyes were kept moist with artificial tears during imaging and the animals were placed on warming pads after imaging until consciousness was regained. Images were captured and saved by the Retinal Imaging System (Micron IV, Phoenix). The integrated curvature and the tortuosity index of fundus images were calculated with ImageJ software as described.[77]

Fluorescence-activated cell sorting

Fresh retinas (six retinas per group) were isolated from mouse eyes, and the single-cell suspensions were generated using the Papain Dissociation System (Worthington BioChem, LK003150). Retina cells were incubated with FITC-CD45 antibody for 30 min on ice in a dark box and washed three times by centrifugation at 1,000 rpm for 3 min, then resuspended cells in ice-cold fluorescence-activated cell sorting buffer containing 5% bovine serum albumin (Invitrogen, AM2616) and 0.5 mM EDTA in PBS. Cells were kept in the dark on ice for sorting. Dead cells were removed using the LIVE/DEAD Fixable Dead Cell Stain Sampler Kit (Invitrogen, L34960) during sorting. CD45-positive cells were collected for scRNA-seq.

Single-cell RNA sequencing and data analysis

Single-cell RNA sequencing (scRNA-seq) was performed by the Translational Immunogenomics Lab (TIGL) at Dana Farber Cancer Institute using the 10x Genomics platform. The raw data were analyzed using the 10x Cellranger pipeline. Sequencing read counts in single cells from three groups were processed and merged for pooled analysis. Doublets, dead cells, and empty droplets were removed, and cells with >500 and <5,000 detected genes, and <8% of transcripts that are of mitochondrial origin were included. Sequentially, the data were normalized using the "LogNormalize" method, 2,000 highly variable features were selected, and the data were centered and scaled by their root-mean-square. PCA analysis was then performed for dimension reduction. The Louvain optimization-based clustering method was used on the top 20 principal components to identify clusters, which were then assigned to cell types based on well-evidenced cell markers. CD45-negative cells were filtered, and $CD45^+$ cells were clustered and focused on the downstream analysis. DotPlots were generated using the "DotPlot" function of Seurat 4.0,[78] which scaled the data to *Z* scores for visualization. Cell clusters were visualized in reduced dimensions of t-distributed stochastic neighbor embedding (tSNE). To compare gene expression between cell types, the Wilcoxon rank-sum test was used, and the Bonferroni method was applied to adjust p values to control false positives due to multiple comparisons. SCANNER[79] was used for data visualization and exploration. The software and algorithms used in this study are listed in Table S2.

Pathway analysis

The Escape package[80] was utilized to perform Gene Set Enrichment Analysis (GSEA) pathway analysis.[81] Pathways were downloaded from the Molecular Signatures Database (https://www.gsea-msigdb.org/gsea/msigdb/) to perform the enrichment analysis for *Socs3 f/f* normal, *Socs3 f/f* OIR, and *Socs3 cKO* OIR datasets. The results were visualized by exporting the pathways activity scores and utilizing ggplot2 geom_histogram() function.

RNA velocity analysis

The RNA velocity analysis was performed using Cellranger, samtools, velocyto, and scvelo packages.[35] By using the Cellranger count function on.fastq files in Ubuntu WSL 20.04, a Cellranger output folder was generated. The samtools sort function was used in the samtools package (-t CB -O BAM) to create the cellsorted_possorted_genome_bam.bam file from the possorted_genome_bam.bam file. The generated file was used for making the.loom file upon utilizing the velocyto run10x function of the velocyto package. The reference genome used for generating the.loom file is GENCODE (https://www.gencodegenes.org/) annotation v.M27, and the repeat annotation for the reference genome was obtained from the UCSC genome browser in.gtf format. Once the.loom file is generated, the.h5Seurat annotated objects were converted to.h5ad objects to transfer them from R to the Python environment. The scVelo package[82] for the RNA velocity analysis was used. The.loom files with the respective data files previously generated were merged, processed, and annotated. The following files were filtered and normalized. First- and second-order moments (means and uncentered variances) were computed among nearest neighbors in PCA space with the scvelo.pp.moments() function. Then velocity (scvelo.tl.velocity()) was estimated, the velocity_graph (scvelo.tl.velocity_graph()) was built, and velocities were projected using scvelo.pl.velocity_embedding_stream() and scvelo.pl.velocity_embedding_grid() on ForceAtlas2 (basis = 'draw_graph_fa') embedding. The software and algorithms are listed in Table S2.

CellChat analysis

The CellChat package[37] was used to extract information related to incoming and outgoing cluster ligand-receptor interactions. Seurat objects and the standard pipeline were used for analysis (https://github.com/sqjin/CellChat/blob/master/tutorial/CellChat-vignette.html). To avoid the projection reducing the dropout effects of signaling genes, in particular for possible zero expression of subunits of ligands/receptors, the raw.use = FALSE setting in computeCommunProb function was used. The population.size = TRUE parameter was used to consider the effect of cell proportion in each cell group during probability calculation. The software and algorithms used in this study are listed in Table S2.

Magnetic-activated cell sorting

Fresh retinas were isolated from mouse eyes and a single-cell suspension was generated by the Papain Dissociation System (Worthington BioChem, LK003150). Cells were passed through a 70 μM nylon mesh (Falcon, 352350), pelleted by centrifugation at 300 × *g* for 10 min, and resuspended in a degassed working solution containing PBS (pH 7.2), 0.5% bovine serum albumin (Invitrogen, AM2616), and 2 mM EDTA. CD45 microbeads (Miltenyi Biotec, 130-052-301) were incubated with the cells for 15 min at 4°C. After incubation, cells were washed and resuspended to a concentration of 10^8 cells per 500 μl working solution. MS columns (Miltenyi Biotec, 130-042-201) were mounted onto the MiniMACS (Miltenyi Biotec, 130-042-102) magnetic separator and rinsed with working solution before loading single-cell suspensions. Unlabeled cells were washed three times with 500 μl working solution and collected. The MS columns were then removed from the MiniMACS separator, and 1 mL working solution was added to the columns. Magnetically labeled $CD45^+$ cell fractions were immediately flushed out of the column with a plunger and collected.

Total RNA extraction and quantitative real-time-PCR

$CD45^+$ immune cells isolated from mouse retinas were used for total RNA extraction using a kit (Zymo Research, R1054) following the manufacturer's instructions. The total RNA was used for cDNA synthesis using the iScript cDNA Synthesis Kit (Bio-Rad, 1708890). The cDNA was then used for quantitative real-time PCR using SYBR Green (Apex Bio, K1070), with *Cyclophilin A* as an internal control for murine samples. The PCR primer sequences are listed in Table S3.

Laser-induced CNV mouse model

The laser-induced CNV mouse model was performed as described.[83] Briefly, ~6- to 8-week-old mice were anesthetized using a ketamine/xylazine solution via intraperitoneal injection, followed by pupil dilation with 1% tropicamide. Laser burns were induced using an image-guided laser system (Micron IV, Phoenix) in the mouse eye. Mice were euthanized at the indicated time points after laser exposure, and mouse eyes were fixed in 4% paraformaldehyde (Fisher Scientific, AAJ19943K2) in 10 mM PBS for 1 h. The retinal pigment epithelium-sclera-choroid complex was dissected, permeabilized with 0.2% Triton X-100 in 10 mM PBS for 1 h, stained with the indicated antibodies, and flat-mounted onto slides using mounting medium (Vector Labs, H-1000-10) after washing with PBS. The flat-mount images were taken using AxioObserver.Z1 microscope (Zeiss) or confocal microscope (Zeiss, LSM700 or LSM980). The CNV lesions were quantified using ImageJ by masked researchers. Exclusion criteria for laser-induced CNV lesions were used as described.[83]

Luciferase reporter constructs preparation and luciferase reporter assay

DNA fragments containing putative STAT3 binding sites on the *Spp1* promoter regions, including promoter 2.6k (P2.6K), enhancer 1 (E1), and enhancer 2 (E2), were amplified from mouse genomic DNA with primers and cloned into the luciferase report vector pTA-Luc (Clontech) to generate *Spp1* luciferase reporter constructs. Mutant constructs of the *Spp1* luciferase reporters with deletions of STAT3 binding sites were constructed with mutagenesis primers for each binding site. HEK293T cells (ATCC, CRL-3216) were transiently transfected with the STAT3-expressing plasmid and wild-type or mutant pTA-Luc-*Spp1* luciferase reporters. Renilla luciferase vector alone was used as a control. At 36 h post-transfection, cells were lysed in passive lysis buffer in the dual-luciferase assay system (Promega, E2920), and luciferase reporter activities were measured using an EnSight Multimode Plate Reader (PerkinElmer luminometer). The primer sequences for luciferase reporters are listed in Table S4.

Treatment with reagents for SOCS3 activation and SPP1 blocking

Naringenin (400 mg/kg/d, gavage)[26] and control reagents were administrated to C57BL/6J OIR mice from P12 to P16. SOCS3 peptidomimetic and negative control peptides were synthesized and purified as below. Solvents were obtained from Romil (Dublin, Ireland). Reverse-phase columns and the LC-MS system were obtained from ThermoFisher (Waltham, MA). The building block Fmoc-NH-(PEG)-COOH (nine atoms) served as PEG moiety. To aid cellular penetration, the cell penetrating peptide (CPP)-Tat (48–60 fragment of HIV Tat protein, GRKKRRQRRRPQGG), carrying fluorescein isothiocyanate as fluorophore, was conjugated to SOCS3 mimetic and negative control peptide. Crude products were purified through reversed-phase HPLC, applying a linear gradient of CH_3CN to water, both with 0.1% TFA, from 5% to 70% over 15 min, using a 2.2 × 5 cm C18 column at a flow rate of 20 mL/min and a UV detector at a wavelength of 210 nm. The identity and purity of main products were evaluated by LC-MS, and purified compounds were lyophilized and stored at −20°C until use. Purified compounds were diluted into PBS to a final concentration of 10 μg/μL prior to injections. SOCS3 peptidomimetic and negative control peptides were administered intraperitoneally into mice with OIR at a dose of 10 mg/kg from P13 to P16. Mouse SPP1 neutralizing antibody (R&D Systems, AF808) and goat immunoglobulin G (IgG) control antibody (R&D Systems, AB-109-C) were diluted into sterile PBS to a concentration of 1 μg/μL. One microgram of SPP1 neutralizing antibody or IgG was intravitreally injected into each eye of OIR mice at P14.

Statistics

GraphPad Prism was used for statistical analyses. Results are presented as means ± standard error of the mean. All experiments were repeated independently at least three times. Unpaired nonparametric Mann-Whitney test was used for two-group comparison. Unpaired nonparametric Kruskai-Wallis Dunn's multiple comparisons test was used for multiple-group comparison. Hypergeometric enrichment analysis was performed with the phyper function in the R stats package. Enrichment was considered significant at the $\alpha = 0.05$ level with a Bonferroni correction for testing multiple hypotheses. p values <0.05 were considered statistically significant.

DATA AND CODE AVAILABILITY

The scRNA-seq datasets have been deposited in the Genome Expression Omnibus (GEO) under the accession numbers (GSE227861). The code and processed annotated datasets generated in this study for reproducing the bioinformatical analysis can be found on the following GitHub repository: https://github.com/mcrewcow/Sun_Ye_microglia_macrophages_paper. GSE86169[40] and GSE1 88145[41] are available through the original publications. All datasets generated are available from the corresponding author upon request. All other data are provided in the main text or the supplemental information.

SUPPLEMENTAL INFORMATION

Supplemental information can be found online at https://doi.org/10.1016/j.ymthe.2024.03.025.

ACKNOWLEDGMENTS

We thank Dr. Lois E.H. Smith for her expert advice on ROP treatment and critical review of the manuscript. We thank Dr. Jing Chen for her insightful advice on the manuscript. We thank Dr. Shuqiang Li from the Translational Immunogenomics Lab (TIGL) at Dana Farber Cancer Institute for the preliminary analysis of scRNA-seq data using the 10x Cellranger pipeline. We thank Dr. Ronald Mathieu from the Flow

Cytometry Core at Boston Children's Hospital for providing technical support on cell sorting. We thank the IDDRC Cellular Imaging Core, funded by NIH P50 HD105351 and NIH S10D030322, for imaging support. This work was supported by the National Institutes of Health (R01EY030140, R01EY029238), BrightFocus Foundation, Mass Lions Eye Research Fund, Boston Children's Hospital Pilot Fund, and Children's Hospital Ophthalmology Foundation for Y.S.; Knights Templar Eye Foundation for T.W.; National Institutes of Health (R01HL146128) for S.K.; Associazione Italiana per la Ricerca sul Cancro (AIRC) grant (IG 2022, Rif. 27378) for D.M.; Medical Research Council (United Kingdom) (MR/W004681/1) for H.X.; National Institutes of Health/National Eye Institute (U24EY029893) and Gilbert Family Foundation for P.B..

AUTHOR CONTRIBUTIONS

Y.S. and T.W. conceived and designed the study. G.C., P.B., A.S., H.X., and U.H.A. assisted in the design. T.W., S.K., D.A., E.L., Y.W., and Y.S. conducted the experiments using mouse models. S.L. and D.M. synthesized the peptides. E.K., P.B., and G.C. conducted the single-cell RNA sequencing data analysis. A.F.-G., S.A.M., and S.K. conducted the experiments using an oxygen chamber. M.C. and H.X. conducted the experiments using human samples. T.W., S.K., D.A., A.S., M.C., H.X., and Y.S. analyzed the data. G.C. reviewed all the statistical analysis. T.W., S.K., E.K., and Y.S. drafted the manuscript. All authors were involved in the interpretation and critical review of the data and reviewed the final version of the manuscript.

DECLARATION OF INTERESTS

Y.S. and T.W. are inventors on patent applications relating to this work filed by Boston Children's Hospital.

REFERENCES

1. Wang, Q., Zheng, J., Pettersson, S., Reynolds, R., and Tan, E.K. (2023). The link between neuroinflammation and the neurovascular unit in synucleinopathies. Sci. Adv. *9*, eabq1141. https://doi.org/10.1126/sciadv.abq1141.

2. Iadecola, C. (2017). The Neurovascular Unit Coming of Age: A Journey through Neurovascular Coupling in Health and Disease. Neuron *96*, 17–42. https://doi.org/10.1016/j.neuron.2017.07.030.

3. Fantin, A., Vieira, J.M., Gestri, G., Denti, L., Schwarz, Q., Prykhozhij, S., Peri, F., Wilson, S.W., and Ruhrberg, C. (2010). Tissue macrophages act as cellular chaperones for vascular anastomosis downstream of VEGF-mediated endothelial tip cell induction. Blood *116*, 829–840. https://doi.org/10.1182/blood-2009-12-257832.

4. Haruwaka, K., Ikegami, A., Tachibana, Y., Ohno, N., Konishi, H., Hashimoto, A., Matsumoto, M., Kato, D., Ono, R., Kiyama, H., et al. (2019). Dual microglia effects on blood brain barrier permeability induced by systemic inflammation. Nat. Commun. *10*, 5816. https://doi.org/10.1038/s41467-019-13812-z.

5. Hartnett, M.E., and Penn, J.S. (2013). Mechanisms and management of retinopathy of prematurity. N. Engl. J. Med. *368*, 1162–1163. https://doi.org/10.1056/NEJMc1301021.

6. Tasman, W., Patz, A., McNamara, J.A., Kaiser, R.S., Trese, M.T., and Smith, B.T. (2006). Retinopathy of prematurity: the life of a lifetime disease. Am. J. Ophthalmol. *141*, 167–174. https://doi.org/10.1016/j.ajo.2005.07.034.

7. Blencowe, H., Cousens, S., Oestergaard, M.Z., Chou, D., Moller, A.B., Narwal, R., Adler, A., Vera Garcia, C., Rohde, S., Say, L., and Lawn, J.E. (2012). National, regional, and worldwide estimates of preterm birth rates in the year 2010 with time trends since 1990 for selected countries: a systematic analysis and implications. Lancet *379*, 2162–2172. https://doi.org/10.1016/S0140-6736(12)60820-4.

8. Yonekawa, Y., Miller, J.W., and Kim, I.K. (2015). Age-Related Macular Degeneration: Advances in Management and Diagnosis. J. Clin. Med. *4*, 343–359. https://doi.org/10.3390/jcm4020343.

9. Tolsma, K.W., Allred, E.N., Chen, M.L., Duker, J., Leviton, A., and Dammann, O. (2011). Neonatal bacteremia and retinopathy of prematurity: the ELGAN study. Arch. Ophthalmol. *129*, 1555–1563. https://doi.org/10.1001/archophthalmol.2011.319.

10. Chen, M., Citil, A., McCabe, F., Leicht, K.M., Fiascone, J., Dammann, C.E.L., and Dammann, O. (2011). Infection, oxygen, and immaturity: interacting risk factors for retinopathy of prematurity. Neonatology *99*, 125–132. https://doi.org/10.1159/000312821.

11. Polam, S., Koons, A., Anwar, M., Shen-Schwarz, S., and Hegyi, T. (2005). Effect of chorioamnionitis on neurodevelopmental outcome in preterm infants. Arch. Pediatr. Adolesc. Med. *159*, 1032–1035. https://doi.org/10.1001/archpedi.159.11.1032.

12. Moscuzza, F., Belcari, F., Nardini, V., Bartoli, A., Domenici, C., Cuttano, A., Ghirri, P., and Boldrini, A. (2011). Correlation between placental histopathology and fetal/neonatal outcome: chorioamnionitis and funisitis are associated to intraventricular haemorrage and retinopathy of prematurity in preterm newborns. Gynecol. Endocrinol. *27*, 319–323. https://doi.org/10.3109/09513590.2010.487619.

13. Lee, J., and Dammann, O. (2012). Perinatal infection, inflammation, and retinopathy of prematurity. Semin. Fetal Neonatal. Med. *17*, 26–29. https://doi.org/10.1016/j.siny.2011.08.007.

14. Dammann, O. (2010). Inflammation and retinopathy of prematurity. Acta Paediatr. *99*, 975–977. https://doi.org/10.1111/j.1651-2227.2010.01836.x.

15. Hong, H.K., Lee, H.J., Ko, J.H., Park, J.H., Park, J.Y., Choi, C.W., Yoon, C.H., Ahn, S.J., Park, K.H., Woo, S.J., and Oh, J.Y. (2014). Neonatal systemic inflammation in rats alters retinal vessel development and simulates pathologic features of retinopathy of prematurity. J. Neuroinflammation *11*, 87. https://doi.org/10.1186/1742-2094-11-87.

16. Dammann, O., Brinkhaus, M.J., Bartels, D.B., Dördelmann, M., Dressler, F., Kerk, J., Dörk, T., and Dammann, C.E.L. (2009). Immaturity, perinatal inflammation, and retinopathy of prematurity: a multi-hit hypothesis. Early Hum. Dev. *85*, 325–329. https://doi.org/10.1016/j.earlhumdev.2008.12.010.

17. Carow, B., and Rottenberg, M.E. (2014). SOCS3, a Major Regulator of Infection and Inflammation. Front. Immunol. *5*, 58. https://doi.org/10.3389/fimmu.2014.00058.

18. Ushiki, T., Huntington, N.D., Glaser, S.P., Kiu, H., Georgiou, A., Zhang, J.G., Metcalf, D., Nicola, N.A., Roberts, A.W., and Alexander, W.S. (2016). Rapid Inflammation in Mice Lacking Both SOCS1 and SOCS3 in Hematopoietic Cells. PLoS One *11*, e0162111. https://doi.org/10.1371/journal.pone.0162111.

19. Qin, H., Holdbrooks, A.T., Liu, Y., Reynolds, S.L., Yanagisawa, L.L., and Benveniste, E.N. (2012). SOCS3 deficiency promotes M1 macrophage polarization and inflammation. J. Immunol. *189*, 3439–3448. https://doi.org/10.4049/jimmunol.1201168.

20. Arnold, C.E., Whyte, C.S., Gordon, P., Barker, R.N., Rees, A.J., and Wilson, H.M. (2014). A critical role for SOCS3 in promoting M1 macrophage activation and function *in vitro* and *in vivo*. Immunology *141*, 96–110. https://doi.org/10.1111/imm.12173.

21. Stahl, A., Joyal, J.S., Chen, J., Sapieha, P., Juan, A.M., Hatton, C.J., Pei, D.T., Hurst, C.G., Seaward, M.R., Krah, N.M., et al. (2012). SOCS3 is an endogenous inhibitor of pathologic angiogenesis. Blood *120*, 2925–2929. https://doi.org/10.1182/blood-2012-04-422527.

22. Sun, Y., Ju, M., Lin, Z., Fredrick, T.W., Evans, L.P., Tian, K.T., Saba, N.J., Morss, P.C., Pu, W.T., Chen, J., et al. (2015). SOCS3 in retinal neurons and glial cells suppresses VEGF signaling to prevent pathological neovascular growth. Sci. Signal. *8*, ra94. https://doi.org/10.1126/scisignal.aaa8695.

23. Sun, Y., Liu, C.H., SanGiovanni, J.P., Evans, L.P., Tian, K.T., Zhang, B., Stahl, A., Pu, W.T., Kamenecka, T.M., Solt, L.A., and Chen, J. (2015). Nuclear receptor RORalpha regulates pathologic retinal angiogenesis by modulating SOCS3-dependent inflammation. Proc. Natl. Acad. Sci. USA *112*, 10401–10406. https://doi.org/10.1073/pnas.1504387112.

24. Hombrebueno, J.R., Lynch, A., Byrne, E.M., Obasanmi, G., Kissenpfennig, A., Chen, M., and Xu, H. (2020). Hyaloid Vasculature as a Major Source of STAT3(+) (Signal Transducer and Activator of Transcription 3) Myeloid Cells for Pathogenic Retinal

Neovascularization in Oxygen-Induced Retinopathy. Arterioscler. Thromb. Vasc. Biol. *40*, e367–e379. https://doi.org/10.1161/ATVBAHA.120.314567.

25. Smith, L.E., Wesolowski, E., McLellan, A., Kostyk, S.K., D'Amato, R., Sullivan, R., and D'Amore, P.A. (1994). Oxygen-induced retinopathy in the mouse. Invest. Ophthalmol. Vis. Sci. *35*, 101–111.

26. Wang, T., Zhou, P., Xie, X., Tomita, Y., Cho, S., Tsirukis, D., Lam, E., Luo, H.R., and Sun, Y. (2021). Myeloid lineage contributes to pathological choroidal neovascularization formation via SOCS3. EBioMedicine *73*, 103632. https://doi.org/10.1016/j.ebiom.2021.103632.

27. Ashkar, S., Weber, G.F., Panoutsakopoulou, V., Sanchirico, M.E., Jansson, M., Zawaideh, S., Rittling, S.R., Denhardt, D.T., Glimcher, M.J., and Cantor, H. (2000). Eta-1 (osteopontin): an early component of type-1 (cell-mediated) immunity. Science *287*, 860–864. https://doi.org/10.1126/science.287.5454.860.

28. Schlecht, A., Zhang, P., Wolf, J., Thien, A., Rosmus, D.D., Boneva, S., Schlunck, G., Lange, C., and Wieghofer, P. (2020). Secreted Phosphoprotein 1 Expression in Retinal Mononuclear Phagocytes Links Murine to Human Choroidal Neovascularization. Front. Cell Dev. Biol. *8*, 618598. https://doi.org/10.3389/fcell.2020.618598.

29. Macosko, E.Z., Basu, A., Satija, R., Nemesh, J., Shekhar, K., Goldman, M., Tirosh, I., Bialas, A.R., Kamitaki, N., Martersteck, E.M., et al. (2015). Highly Parallel Genome-wide Expression Profiling of Individual Cells Using Nanoliter Droplets. Cell *161*, 1202–1214. https://doi.org/10.1016/j.cell.2015.05.002.

30. Masuda, T., Sankowski, R., Staszewski, O., and Prinz, M. (2020). Microglia Heterogeneity in the Single-Cell Era. Cell Rep. *30*, 1271–1281. https://doi.org/10.1016/j.celrep.2020.01.010.

31. Dermitzakis, I., Theotokis, P., Evangelidis, P., Delilampou, E., Evangelidis, N., Chatzisavvidou, A., Avramidou, E., and Manthou, M.E. (2023). CNS Border-Associated Macrophages: Ontogeny and Potential Implication in Disease. Curr. Issues Mol. Biol. *45*, 4285–4300. https://doi.org/10.3390/cimb45050272.

32. Droho, S., Rajesh, A., Cuda, C.M., Perlman, H., and Lavine, J.A. (2023). CD11c+ macrophages are proangiogenic and necessary for experimental choroidal neovascularization. JCI Insight *8*, e168142. https://doi.org/10.1172/jci.insight.168142.

33. Liu, Z., Shi, H., Xu, J., Yang, Q., Ma, Q., Mao, X., Xu, Z., Zhou, Y., Da, Q., Cai, Y., et al. (2022). Single-cell transcriptome analyses reveal microglia types associated with proliferative retinopathy. JCI Insight *7*, e160940. https://doi.org/10.1172/jci.insight.160940.

34. Lidgerwood, G.E., Senabouth, A., Smith-Anttila, C.J.A., Gnanasambandapillai, V., Kaczorowski, D.C., Amann-Zalcenstein, D., Fletcher, E.L., Naik, S.H., Hewitt, A.W., Powell, J.E., and Pébay, A. (2021). Transcriptomic Profiling of Human Pluripotent Stem Cell-derived Retinal Pigment Epithelium over Time. Dev. Reprod. Biol. *19*, 223–242. https://doi.org/10.1016/j.gpb.2020.08.002.

35. La Manno, G., Soldatov, R., Zeisel, A., Braun, E., Hochgerner, H., Petukhov, V., Lidschreiber, K., Kastriti, M.E., Lönnerberg, P., Furlan, A., et al. (2018). RNA velocity of single cells. Nature *560*, 494–498. https://doi.org/10.1038/s41586-018-0414-6.

36. Wieghofer, P., Knobeloch, K.P., and Prinz, M. (2015). Genetic targeting of microglia. Glia *63*, 1–22. https://doi.org/10.1002/glia.22727.

37. Jin, S., Guerrero-Juarez, C.F., Zhang, L., Chang, I., Ramos, R., Kuan, C.H., Myung, P., Plikus, M.V., and Nie, Q. (2021). Inference and analysis of cell-cell communication using CellChat. Nat. Commun. *12*, 1088. https://doi.org/10.1038/s41467-021-21246-9.

38. Stahl, A., Connor, K.M., Sapieha, P., Chen, J., Dennison, R.J., Krah, N.M., Seaward, M.R., Willett, K.L., Aderman, C.M., Guerin, K.I., et al. (2010). The mouse retina as an angiogenesis model. Invest. Ophthalmol. Vis. Sci. *51*, 2813–2826. https://doi.org/10.1167/iovs.10-5176.

39. Ritter, M.R., Banin, E., Moreno, S.K., Aguilar, E., Dorrell, M.I., and Friedlander, M. (2006). Myeloid progenitors differentiate into microglia and promote vascular repair in a model of ischemic retinopathy. J. Clin. Invest. *116*, 3266–3276. https://doi.org/10.1172/JCI29683.

40. Conaway, E.A., de Oliveira, D.C., McInnis, C.M., Snapper, S.B., and Horwitz, B.H. (2017). Inhibition of Inflammatory Gene Transcription by IL-10 Is Associated with Rapid Suppression of Lipopolysaccharide-Induced Enhancer Activation. J. Immunol. *198*, 2906–2915. https://doi.org/10.4049/jimmunol.1601781.

41. ENCODE Project Consortium (2012). An integrated encyclopedia of DNA elements in the human genome. Nature *489*, 57–74. https://doi.org/10.1038/nature11247.

42. Song, M.M., and Shuai, K. (1998). The suppressor of cytokine signaling (SOCS) 1 and SOCS3 but not SOCS2 proteins inhibit interferon-mediated antiviral and antiproliferative activities. J. Biol. Chem. *273*, 35056–35062. https://doi.org/10.1074/jbc.273.52.35056.

43. Wu, L.H., Lin, C., Lin, H.Y., Liu, Y.S., Wu, C.Y.J., Tsai, C.F., Chang, P.C., Yeh, W.L., and Lu, D.Y. (2016). Naringenin Suppresses Neuroinflammatory Responses Through Inducing Suppressor of Cytokine Signaling 3 Expression. Mol. Neurobiol. *53*, 1080–1091. https://doi.org/10.1007/s12035-014-9042-9.

44. Wiejak, J., Dunlop, J., Mackay, S.P., and Yarwood, S.J. (2013). Flavanoids induce expression of the suppressor of cytokine signalling 3 (SOCS3) gene and suppress IL-6-activated signal transducer and activator of transcription 3 (STAT3) activation in vascular endothelial cells. Biochem. J. *454*, 283–293. https://doi.org/10.1042/BJ20130481.

45. La Manna, S., Lee, E., Ouzounova, M., Di Natale, C., Novellino, E., Merlino, A., Korkaya, H., and Marasco, D. (2018). Mimetics of suppressor of cytokine signaling 3: Novel potential therapeutics in triple breast cancer. Int. J. Cancer *143*, 2177–2186. https://doi.org/10.1002/ijc.31594.

46. La Manna, S., Lopez-Sanz, L., Mercurio, F.A., Fortuna, S., Leone, M., Gomez-Guerrero, C., and Marasco, D. (2020). Chimeric peptidomimetics of SOCS 3 able to interact with JAK2 as anti-inflammatory compounds. ACS Med. Chem. Lett. *11*, 615–623.

47. La Manna, S., Leone, M., Mercurio, F.A., Florio, D., and Marasco, D. (2022). Structure-Activity Relationship Investigations of Novel Constrained Chimeric Peptidomimetics of SOCS3 Protein Targeting JAK2. Pharmaceuticals (Basel) *15*, 458. https://doi.org/10.3390/ph15040458.

48. Binet, F., Cagnone, G., Crespo-Garcia, S., Hata, M., Neault, M., Dejda, A., Wilson, A.M., Buscarlet, M., Mawambo, G.T., Howard, J.P., et al. (2020). Neutrophil extracellular traps target senescent vasculature for tissue remodeling in retinopathy. Science *369*, eaay5356. https://doi.org/10.1126/science.aay5356.

49. Santos, A.M., Calvente, R., Tassi, M., Carrasco, M.C., Martín-Oliva, D., Marín-Teva, J.L., Navascués, J., and Cuadros, M.A. (2008). Embryonic and postnatal development of microglial cells in the mouse retina. J. Comp. Neurol. *506*, 224–239. https://doi.org/10.1002/cne.21538.

50. Chen, L., Yang, P., and Kijlstra, A. (2002). Distribution, markers, and functions of retinal microglia. Ocul. Immunol. Inflamm. *10*, 27–39. https://doi.org/10.1076/ocii.10.1.27.10328.

51. Stefater, J.A., 3rd, Lewkowich, I., Rao, S., Mariggi, G., Carpenter, A.C., Burr, A.R., Fan, J., Ajima, R., Molkentin, J.D., Williams, B.O., et al. (2011). Regulation of angiogenesis by a non-canonical Wnt-Flt1 pathway in myeloid cells. Nature *474*, 511–515. https://doi.org/10.1038/nature10085.

52. Checchin, D., Sennlaub, F., Levavasseur, E., Leduc, M., and Chemtob, S. (2006). Potential role of microglia in retinal blood vessel formation. Invest. Ophthalmol. Vis. Sci. *47*, 3595–3602. https://doi.org/10.1167/iovs.05-1522.

53. He, C., Liu, Y., Huang, Z., Yang, Z., Zhou, T., Liu, S., Hao, Z., Wang, J., Feng, Q., Liu, Y., et al. (2021). A specific RIP3(+) subpopulation of microglia promotes retinopathy through a hypoxia-triggered necroptotic mechanism. Proc. Natl. Acad. Sci. USA *118*, e2023290118. https://doi.org/10.1073/pnas.2023290118.

54. Chiang, M.F., Quinn, G.E., Fielder, A.R., Ostmo, S.R., Paul Chan, R.V., Berrocal, A., Binenbaum, G., Blair, M., Peter Campbell, J., Capone, A., Jr., et al. (2021). International Classification of Retinopathy of Prematurity, Third Edition. Ophthalmology *128*, e51–e68. https://doi.org/10.1016/j.ophtha.2021.05.031.

55. Quinn, G.E., Schaffer, D.B., and Johnson, L. (1982). A revised classification of retinopathy of prematurity. Am. J. Ophthalmol. *94*, 744–749. https://doi.org/10.1016/0002-9394(82)90298-7.

56. Keren-Shaul, H., Spinrad, A., Weiner, A., Matcovitch-Natan, O., Dvir-Szternfeld, R., Ulland, T.K., David, E., Baruch, K., Lara-Astaiso, D., Toth, B., et al. (2017). A Unique Microglia Type Associated with Restricting Development of Alzheimer's Disease. Cell *169*, 1276–1290.e17. https://doi.org/10.1016/j.cell.2017.05.018.

57. Deczkowska, A., Keren-Shaul, H., Weiner, A., Colonna, M., Schwartz, M., and Amit, I. (2018). Disease-Associated Microglia: A Universal Immune Sensor of Neurodegeneration. Cell *173*, 1073–1081. https://doi.org/10.1016/j.cell.2018.05.003.

58. Silvin, A., Uderhardt, S., Piot, C., Da Mesquita, S., Yang, K., Geirsdottir, L., Mulder, K., Eyal, D., Liu, Z., Bridlance, C., et al. (2022). Dual ontogeny of disease-associated microglia and disease inflammatory macrophages in aging and neurodegeneration. Immunity *55*, 1448–1465.e6. https://doi.org/10.1016/j.immuni.2022.07.004.

59. Droho, S., Voigt, A.P., Sterling, J.K., Rajesh, A., Chan, K.S., Cuda, C.M., Perlman, H., and Lavine, J.A. (2023). NR4A1 deletion promotes pro-angiogenic polarization of macrophages derived from classical monocytes in a mouse model of neovascular age-related macular degeneration. J. Neuroinflammation *20*, 238. https://doi.org/10.1186/s12974-023-02928-1.

60. Duan, X., Qiao, M., Bei, F., Kim, I.J., He, Z., and Sanes, J.R. (2015). Subtype-specific regeneration of retinal ganglion cells following axotomy: effects of osteopontin and mTOR signaling. Neuron *85*, 1244–1256. https://doi.org/10.1016/j.neuron.2015.02.017.

61. Li, S., and Jakobs, T.C. (2022). Secreted phosphoprotein 1 slows neurodegeneration and rescues visual function in mouse models of aging and glaucoma. Cell Rep. *41*, 111880. https://doi.org/10.1016/j.celrep.2022.111880.

62. Tu, W., Zheng, H., Li, L., Zhou, C., Feng, M., Chen, L., Li, D., Chen, X., Hao, B., Sun, H., et al. (2022). Secreted phosphoprotein 1 promotes angiogenesis of glioblastoma through upregulating PSMA expression via transcription factor HIF-1alpha. Acta Biochim. Biophys. Sin. *55*, 417–425. https://doi.org/10.3724/abbs.2022157.

63. Bai, Q., Wang, X., Yan, H., Wen, L., Zhou, Z., Ye, Y., Jing, Y., Niu, Y., Wang, L., Zhang, Z., et al. (2023). Microglia-Derived Spp1 Promotes Pathological Retinal Neovascularization via Activating Endothelial Kit/Akt/mTOR Signaling. J. Pers. Med. *13*, 146. https://doi.org/10.3390/jpm13010146.

64. Wang, D., Yamamoto, S., Hijiya, N., Benveniste, E.N., and Gladson, C.L. (2000). Transcriptional regulation of the human osteopontin promoter: functional analysis and DNA-protein interactions. Oncogene *19*, 5801–5809. https://doi.org/10.1038/sj.onc.1203917.

65. Wai, P.Y., Mi, Z., Gao, C., Guo, H., Marroquin, C., and Kuo, P.C. (2006). Ets-1 and runx2 regulate transcription of a metastatic gene, osteopontin, in murine colorectal cancer cells. J. Biol. Chem. *281*, 18973–18982. https://doi.org/10.1074/jbc.M511962200.

66. Schultz, J., Lorenz, P., Ibrahim, S.M., Kundt, G., Gross, G., and Kunz, M. (2009). The functional -443T/C osteopontin promoter polymorphism influences osteopontin gene expression in melanoma cells via binding of c-Myb transcription factor. Mol. Carcinog. *48*, 14–23. https://doi.org/10.1002/mc.20452.

67. Liu, Y.N., Kang, B.B., and Chen, J.H. (2004). Transcriptional regulation of human osteopontin promoter by C/EBPalpha and AML-1 in metastatic cancer cells. Oncogene *23*, 278–288. https://doi.org/10.1038/sj.onc.1207022.

68. Grubman, A., Choo, X.Y., Chew, G., Ouyang, J.F., Sun, G., Croft, N.P., Rossello, F.J., Simmons, R., Buckberry, S., Landin, D.V., et al. (2021). Transcriptional signature in microglia associated with Abeta plaque phagocytosis. Nat. Commun. *12*, 3015. https://doi.org/10.1038/s41467-021-23111-1.

69. Beguier, F., Housset, M., Roubeix, C., Augustin, S., Zagar, Y., Nous, C., Mathis, T., Eandi, C., Benchaboune, M., Drame-Maigné, A., et al. (2020). The 10q26 Risk Haplotype of Age-Related Macular Degeneration Aggravates Subretinal Inflammation by Impairing Monocyte Elimination. Immunity *53*, 429–441.e8. https://doi.org/10.1016/j.immuni.2020.07.021.

70. Fujita, N., Fujita, S., Ogata, N., Matsuoka, M., Okada, Y., Kon, S., Uede, T., and Saika, S. (2011). Endogenous osteopontin involvement in laser-induced choroidal neovascularization in mice. Invest. Ophthalmol. Vis. Sci. *52*, 9310–9315. https://doi.org/10.1167/iovs.10-7050.

71. Fouda, A.Y., Xu, Z., Narayanan, S.P., Caldwell, R.W., and Caldwell, R.B. (2020). Utility of LysM-cre and Cdh5-cre Driver Mice in Retinal and Brain Research: An Imaging Study Using tdTomato Reporter Mouse. Invest. Ophthalmol. Vis. Sci. *61*, 51. https://doi.org/10.1167/iovs.61.3.51.

72. Yasukawa, H., Ohishi, M., Mori, H., Murakami, M., Chinen, T., Aki, D., Hanada, T., Takeda, K., Akira, S., Hoshijima, M., et al. (2003). IL-6 induces an anti-inflammatory response in the absence of SOCS3 in macrophages. Nat. Immunol. *4*, 551–556. https://doi.org/10.1038/ni938.

73. Reed, A.S., Unger, E.K., Olofsson, L.E., Piper, M.L., Myers, M.G., Jr., and Xu, A.W. (2010). Functional role of suppressor of cytokine signaling 3 upregulation in hypothalamic leptin resistance and long-term energy homeostasis. Diabetes *59*, 894–906. https://doi.org/10.2337/db09-1024.

74. Connor, K.M., Krah, N.M., Dennison, R.J., Aderman, C.M., Chen, J., Guerin, K.I., Sapieha, P., Stahl, A., Willett, K.L., and Smith, L.E.H. (2009). Quantification of oxygen-induced retinopathy in the mouse: a model of vessel loss, vessel regrowth and pathological angiogenesis. Nat. Protoc. *4*, 1565–1573. https://doi.org/10.1038/nprot.2009.187.

75. Xiao, S., Bucher, F., Wu, Y., Rokem, A., Lee, C.S., Marra, K.V., Fallon, R., Diaz-Aguilar, S., Aguilar, E., Friedlander, M., and Lee, A.Y. (2017). Fully automated, deep learning segmentation of oxygen-induced retinopathy images. JCI Insight *2*, e97585. https://doi.org/10.1172/jci.insight.97585.

76. Stahl, A., Chen, J., Sapieha, P., Seaward, M.R., Krah, N.M., Dennison, R.J., Favazza, T., Bucher, F., Löfqvist, C., Ong, H., et al. (2010). Postnatal weight gain modifies severity and functional outcome of oxygen-induced proliferative retinopathy. Am. J. Pathol. *177*, 2715–2723. https://doi.org/10.2353/ajpath.2010.100526.

77. Scott, A., Powner, M.B., and Fruttiger, M. (2014). Quantification of vascular tortuosity as an early outcome measure in oxygen induced retinopathy (OIR). Exp. Eye Res. *120*, 55–60. https://doi.org/10.1016/j.exer.2013.12.020.

78. Hao, Y., Hao, S., Andersen-Nissen, E., Mauck, W.M., 3rd, Zheng, S., Butler, A., Lee, M.J., Wilk, A.J., Darby, C., Zager, M., et al. (2021). Integrated analysis of multimodal single-cell data. Cell *184*, 3573–3587.e29. https://doi.org/10.1016/j.cell.2021.04.048.

79. Cai, G., Yu, X., Youn, C., Zhou, J., and Xiao, F. (2022). SCANNER: a web platform for annotation, visualization and sharing of single cell RNA-seq data. Database. (Oxford) *2022*, baab086. https://doi.org/10.1093/database/baab086.

80. Borcherding, N., Vishwakarma, A., Voigt, A.P., Bellizzi, A., Kaplan, J., Nepple, K., Salem, A.K., Jenkins, R.W., Zakharia, Y., and Zhang, W. (2021). Mapping the immune environment in clear cell renal carcinoma by single-cell genomics. Commun. Biol. *4*, 122. https://doi.org/10.1038/s42003-020-01625-6.

81. Subramanian, A., Tamayo, P., Mootha, V.K., Mukherjee, S., Ebert, B.L., Gillette, M.A., Paulovich, A., Pomeroy, S.L., Golub, T.R., Lander, E.S., and Mesirov, J.P. (2005). Gene set enrichment analysis: a knowledge-based approach for interpreting genome-wide expression profiles. Proc. Natl. Acad. Sci. USA *102*, 15545–15550. https://doi.org/10.1073/pnas.0506580102.

82. Bergen, V., Lange, M., Peidli, S., Wolf, F.A., and Theis, F.J. (2020). Generalizing RNA velocity to transient cell states through dynamical modeling. Nat. Biotechnol. *38*, 1408–1414. https://doi.org/10.1038/s41587-020-0591-3.

83. Gong, Y., Li, J., Sun, Y., Fu, Z., Liu, C.H., Evans, L., Tian, K., Saba, N., Fredrick, T., Morss, P., et al. (2015). Optimization of an Image-Guided Laser-Induced Choroidal Neovascularization Model in Mice. PloS one *10*, e0132643. https://doi.org/10.1371/journal.pone.0132643.